

**Key Points:**

- Yield stress and the presence of ACPs alter the frequency of overturn events
- Survival of crustal material during overturn events changes with the presence of ACPs
- ACPs do not seem to be a good representation for Venus' tesserae regions

**Supporting Information:**

- Supporting Information S1

**Correspondence to:**

R. V. M. K. Karlsson and S. C. Werner,  
r.v.m.k.karlsson@geo.uio.no;  
stephanie.werner@geo.uio.no

**Citation:**

Karlsson, R. V. M. K., Cheng, K. W., Cramer, F., Rolf, T., Uppalapati, S., & Werner, S. C. (2020). Implications of anomalous crustal provinces for Venus' resurfacing history. *Journal of Geophysical Research: Planets*, 125, e2019JE006340. <https://doi.org/10.1029/2019JE006340>

Received 19 DEC 2019

Accepted 18 SEP 2020

Accepted article online 23 SEP 2020

## Implications of Anomalous Crustal Provinces for Venus' Resurfacing History

R. V. M. K. Karlsson<sup>1</sup> , K. W. Cheng<sup>2</sup>, F. Cramer<sup>1</sup> , T. Rolf<sup>1</sup>, S. Uppalapati<sup>1</sup> ,  
and S. C. Werner<sup>1</sup> 

<sup>1</sup>Centre for Earth Evolution and Dynamics (CEED), University of Oslo, Oslo, Norway, <sup>2</sup>Department of Earth Sciences, ETH Zurich, Zurich, Switzerland

**Abstract** Current Venus tectonics suggests a stagnant lid mode of mantle convection. However, the planet is debated to enter an episodic regime after long quiescent periods, driven by resurfacing due to rapid subduction and global crustal recycling. Tessera regions that cover approximately 10% of Venus' surface appear to be strongly deformed, which suggests that they have survived at least the latest resurfacing event, although the composition and age of the tesserae are unknown. Based on mantle convection modeling, we studied the effects of anomalous crustal provinces (ACPs) on mantle dynamics and postoverturn lithospheric survival. As a hypothesis, we assume ACPs to be thick, compositionally anomalous, and rheologically strong units, similar to terrestrial cratons. We model Venus with a varying number of preimposed ACP units and differing lithospheric yield stress in 2-D and 3-D spherical geometry. The impact of ACPs on mantle dynamics and the survival of lithosphere is investigated by examining the thermal evolution, crustal thickness, and surface age distribution. We find that the number and timing of overturns are highly dependent on the yield stress and, to some degree, on the number and size of the preimposed ACPs. ACPs in particular affect the wavelength of convection and may foster the survival of lithosphere even of those portions not being part of an ACP. However, ACPs do not seem to be a good analog for tessera regions due to their exaggerated age and (likely) thickness, but—with appropriate density contrast—may be more useful representatives of Venus' highland plateaus.

**Plain Language Summary** Plate tectonics shapes the Earth's surface but is currently probably not active on Venus. Instead, periods with a more mobile Venesian surface remain possible, in particular because the surface is rather young. Episodic resurfacing events—known as overturns—during which much of the surface is recycled into the planetary interior may explain this. However, about 10% of Venus' surface are covered by tesserae, strongly deformed and possibly older-than-average regions that may have survived overturns. The origin of such anomalous crustal provinces (ACPs) is unknown, but we hypothesize them to be similar to the cratonic keels of Earth's continental crust. We investigate how ACPs affect the interior dynamics and resurfacing history and whether they promote the (partial) survival of the surface during overturns. We find that both the presence of ACPs and the strength of the lithosphere alter the overturn frequency. ACPs affect the mantle flow pattern and facilitate survival of non-ACP lithosphere and crust by shielding it from recycling during overturn events. After analyzing our model-predicted distributions of crustal thickness and surface age, however, preexisting ACPs do not seem to be adequate analogues for Venus' tesserae, as their thickness and age appear exaggerated given the observation on Venus' surface.

### 1. Introduction

Venus is very similar to Earth in many aspects (size and bulk composition), yet the two planets differ in a number of ways. Earth has a distinctly dichotomous surface elevation with thick and elevated continents and low-lying oceanic lithosphere, whereas the majority of Venus' surface lies close to the mean planetary elevation. Some areas with higher elevation are the crustal plateaus, which consist of tessera regions that cover 8–10% of the planet (Hansen et al., 2000). They feature high topography, strong deformation, and embayment by volcanic plains (Brown & Grimm, 1997; Ivanov & Head, 2011; Romeo & Turcotte, 2010), so that they might be older than the surrounding areas and therefore hold important information of Venus' resurfacing history.

From the existing observations, little is known about Venus' tesserae. They are rather small areas clustered in three regions, which possibly indicates where they have preferentially formed (Ivanov & Head, 2011). The tesserae have been proposed to be older than the average surface (Ivanov & Basilevsky, 1993; Ogawa & Yanagisawa, 2014), which globally has a nearly uniform age of  $750^{+350}_{-400}$  Myr as constrained by crater densities (McKinnon et al., 1997). However, at least some small portions of the surface are thought to be much younger due to recent volcanic activity (e.g., Smrekar et al., 2010). While the higher age implies that tessera units have experienced a longer history of tectonic activity, crater statistics give little information on their actual age, as the number of craters on any single tessera region is too sparse to reliably suggest surface age differences. Nevertheless, age ranges of 1.0–1.7 times the mean age have been suggested (Ivanov & Basilevsky, 1993; Kreslavsky et al., 2015; Nunes et al., 2004), but these estimates may be lower limits due to the small size of tessera regions.

The composition of the tesserae is not well constrained either but could be more felsic than the mafic (and probably basaltic) composition observed for Venus' plains at most of the Venera landing sites (e.g., Kargel et al., 1993). This is supported by the lower thermal emissivity of these regions (Hashimoto et al., 2008; Romeo & Capote, 2011), although a recent study on the Ovda Regio terrain suggests a closer-to-basaltic composition instead (Wroblewski et al., 2019). Other possible explanations for the observed emissivity anomaly have been proposed (e.g., differences in surface roughness, grain size, or weathering; Basilevsky et al., 2012), but here we pursue the compositional explanation and explore its implications further.

The formation mechanism of Venus' tesserae is still debated. The two principal models are the formation by downwelling of material, causing contraction and crustal thickening (Bindschadler & Head, 1991), versus upwelling of material, causing crustal thickening through volcanic processes (Ghent & Hansen, 1999). Both scenarios involve aspects that cannot be explained by observations: The downwelling model requires too much time for crustal thickening (Kidder & Phillips, 1996), whereas the upwelling model does not explain the large amount of contractional features (Ghent et al., 2005) and the geothermal gradient needed to produce plateaus is much higher than what is expected from an upwelling plume (Gilmore et al., 1998).

Due to these contrasting scenarios and the limited knowledge of age, thickness, and composition, our work does not focus on the formation of crustal plateaus and/or any associated compositional heterogeneity but rather assumes their preexistence. We focus instead on the consequences of such anomalous crustal provinces (hereafter dubbed ACPs) being present. This is done using numerical modeling in analogy to modeling the drift of (similarly compositionally anomalous) continental plates such as Earth's by defining a set of buoyant rheologically strong units (e.g., Lenardic & Moresi, 1999; Rolf & Tackley, 2011). In the terrestrial context, these units represent the continental cratonic roots. For Venus, we assume them to be linked to the observed crustal plateaus, but the effects of such roots on the interior evolution and its surface expressions have never been analyzed as Venus operates in a convectional regime different from Earth's. Earth is in a mobile lid regime with a thin and continuously mobile lithosphere, where the surface is renewed, and heat is lost via plate tectonics. Venus on the other hand may presently operate in a stagnant lid regime in which the planet is covered by one global and almost rigid plate. Heat is lost mainly by volcanic processes, for instance when hot magma pierces through the crust and reaches the surface, perhaps similar to a heat-piping mechanism (Moore & Webb, 2013). However, other tectonic regimes with different styles of ongoing active recycling, even with some variants of subduction, have been proposed for Venus (e.g., Davaille et al., 2017; Sandwell & Schubert, 1992; Smrekar et al., 2010). Because of Venus' rather uniform surface age an alternative is that the planet is in a transitional regime where the stagnant lid is interrupted by periods of surface mobilization (Schaber et al., 1992). This resurfacing mode is called episodic lid, but the absolute need for overturn episodes to explain Venus' observation remains unclear (see e.g., Bjonnes et al., 2012; Ghail, 2015). We explore both end members for resurfacing on Venus in relation to the preimposed anomalous crustal regions and to test how such regions may affect resurfacing.

Specifically, we investigate here how ACPs may affect the internal dynamics of Venus and how this impacts the resurfacing characteristics, in particular how the presence of ACPs alters the signatures of regular surface (away from the ACP) and whether it can grow older crust. Further insight into these questions will support our understanding of Venus' tectonic regime and its evolution. We first introduce our model and define the main diagnostics (section 2). In section 3, we present the main results from our computed models and discuss these in the context of Venus (section 4), before we propose a few key conclusions in section 5.

## 2. Methodology

### 2.1. Numerical Modeling

We adopt the approach of Rolf et al. (2018) and model the evolution of Venus from its early stages until present day. The model features strongly temperature-, pressure-, and strain rate-dependent rheology; phase transitions; and partial melting; for a more detailed description we refer to previous work (Armann & Tackley, 2012; Rolf et al., 2018). To streamline our modeling efforts to the scientific questions introduced above, we made a few simplifications and adjustments compared to these previous works to more efficiently achieve equilibrium states and isolate the processes we are here most interested in.

First, we run most models in 2-D rather than 3-D for reasons of computational feasibility. Second, the internal radiogenic heating is kept constant and uniform throughout the mantle; realistically, it would decrease with time because of the decay of heat producing materials and would be heterogeneously distributed with a higher abundance in the crust. This may affect the thermal structure of the interior including the formation of plumes and the properties of those. Similarly, surface and core-mantle boundary (CMB) temperatures are constant through time while they would change due to interaction with the atmosphere (e.g., Gillmann & Tackley, 2014) and the core (e.g. King, 2018). We do these simplifications because we are mostly interested in Venus' recent history, say the last 1 Gyr. We note that the integration times of our model evolution (shown below) can be much longer than this (e.g., 3 Gyr). This is so, because we want to investigate the characteristic dynamics and a long integration time is needed to get out of an initial transient state and to capture the time scales behind episodic overturns.

Moreover, we preimpose the ACPs, meaning that they are in place at the initiation of the model. The modeled ACPs are highly simplified and can differ from normal material only in terms of density and rheological properties. Each ACP has a strong root and weaker crustal layer on top. The strong root is implemented in such a way that the ACP will not yield and thereby resist subduction. Specifically, the root is 300 times more viscous and has an  $\sim 10^6$  times higher (essentially infinite) surface yield stress than normal material (see below). These extreme contrasts are unlikely to be realistic for actual rocks on Venus' surface, but our motivation for using them is that we want to ensure that ACPs largely resist tectonic deformation and recycling and are stable on the long term. The crustal layer is 0.1 times as viscous as normal material and has the same surface yield stress as the root at the same temperature and depth. The density is typically the same for ACP roots and mantle, although a small density contrast of  $-20 \text{ kg/m}^3$  was added to some models (NC2-YS80 and NC2-YS100), where the ACPs were recycled despite their strong root. For the crustal layer the density contrast is always  $-50 \text{ kg/m}^3$ .

The employed rheology is viscoplastic, such that material deforms purely viscously at stresses below a certain threshold (the yield stress). The viscosity is pressure dependent and highly temperature dependent but does not vary with mineral phase and/or composition except within the ACPs (as described in the previous paragraph). We assume diffusion creep as the only deformation mechanism, not considering other mechanisms like dislocation creep; grain-size variations are also not considered. The vigor of mantle flow in our models is determined by the reference viscosity, which is the viscosity at the reference temperature ( $T_{\text{ref}} = 1,613 \text{ K}$ ) and surface pressure. Here, we adopt a value of  $\eta_{\text{ref}} = 3 \times 10^{20} \text{ Pa s}$ , which is on the order of terrestrial estimates from postglacial rebound for instance (Mitrovica & Forte, 2004).

Upon reaching the yield stress, material fails plastically, which reduces viscosity dramatically and is capable of generating narrow weak zones in the lithosphere (Tackley, 2000) that eventually favor the formation of plate boundaries (in the terrestrial context) or initiates overturn events (in Venus' context). Sticky air is not implemented, so that subduction is double sided rather than one sided as on Earth (Crameri et al., 2012). The yield stress increases from its surface value (YS) toward greater pressure using a friction coefficient of  $\mu = 0.2$ . In our reference model in the stagnant lid regime, we set  $YS = 10^{12} \text{ Pa}$  in order to prevent overturns happening per se. In our main models in the episodic lid regime, however, YS is a free parameter that we vary.

Away from the ACPs, the mantle initially has a homogenous composition and is composed of 80% harzburgite and 20% basalt. The former rock type consists of 75% olivine and 25% pyroxene garnet, while the latter type consists of 100% pyroxene-garnet (see Armann & Tackley, 2012). Both types undergo phase transitions that roughly correspond to the terrestrial transitions at 410 and 660 km depth but happen at somewhat

**Table 1**  
List of Computed 2-D Models Sorted by Yield Stress (YS, in MPa) and the Number of ACPs (NC)

YS $\rightarrow \infty$	NC = 0		NC = 1		NC = 2		NC = 3		NC = 4	
	0	0	0 <sup>(3-D)</sup>	0 <sup>(3-D)</sup>	0	0	0	0	0	0
YS = 150	0	0	1	0.015	0	0	0	0	0	0
YS = 100	2	0.05	2	0.05	0	0	0	0	0	0
YS = 80	3	0.08	3 <sup>(3-D)</sup>	0.09 <sup>(3-D)</sup>	3 <sup>(3-D)</sup>	0.04 <sup>(3-D)</sup>	0	0	0	0
YS = 40	3	0.51	5	0.25	5	0.028	5	0.22	7	0.23

*Note.* The two diagnostics for each parameter combination indicate which cases feature overturns. The value in the left column is the number of distinct overturns. The number in the right column is the total fractional time during which overturns are ongoing (i.e., 0 = continuous stagnant lid and 1 = continuous mobile lid). The three cases that were additionally run in 3-D are marked.

greater depths, as Venus' gravity is weaker than Earth's. The pyroxene-garnet system features an additional transition at shallow depth (~65 km) to account for the transition from basalt to denser eclogite. Each phase transition is associated with a density change and a Clapeyron slope (see Table A1). We do not associate viscosity contrasts with them, for simplicity and because a strong viscosity contrast between upper and lower mantle phases tends to deteriorate the high correlation between topography and geoid as inferred for present-day Venus (Rolf et al., 2018).

While initially homogeneous, material composition can change when partial melting occurs in the interior where the local temperature exceeds the solidus. Basaltic components can partially melt, and the melt is assumed to be strongly buoyant and to rise to the surface. The actual process of rising melt is not modeled here, but the melt is extracted immediately from the mantle and placed upon the surface where it generates new basaltic crust, which parameterizes extrusive volcanism (see Armann & Tackley, 2012; Xie & Tackley, 2004). These processes facilitate the development of a mobile or episodic lid and thus likely affect the stress state in the lithosphere (e.g., Lourenço et al., 2016). Melt is only extracted from the upper mantle (above ~750 km) and would be left alone in the lower mantle. While this reaches too deep in comparison to terrestrial volcanism, the main depth range of melting in our models is only down to ~300–350 km, as this is where the solidus intersects the typical temperature profile (an example profile is given in Figure S1 in the supporting information). Reduction of the maximum extraction depth to more realistic values is thus expected to have little effect. The processes of partial melting and volcanism are important mechanisms for cooling the planetary interior, especially in the absence of efficient surface recycling (e.g., Lourenço et al., 2016; Turcotte, 1989), but we note that all volcanism is assumed to be extrusive: Magmatic intrusions are not considered here for simplicity (Lourenço et al., 2018; cf. Rozel et al., 2017).

## 2.2. Computed Models

Our models are computed with the code StagYY (Hernlund & Tackley, 2008; Tackley, 2008), mostly in 2-D using a spherical annulus geometry (Hernlund & Tackley, 2008; Tackley, 2008) with a resolution of  $512 \times 64$  cells; higher resolutions are also tested and show no first-order differences in the system behavior. The models are set to run for 3.5 Gyr in total, but we emphasize that this time span does not correspond to Venus' evolution since 3.5 Ga due to the model's simplification made above and the unknown initial conditions on Venus. We run the models for several billion years in order to approach an equilibrium state that represents the characteristic system behavior, during which diagnostics like surface age and crustal thickness do no longer change with time systematically. We use  $6.44 \times 10^6$  tracers (~195 per numerical grid cell) that are advected by the predicted flow field and track information about composition using the tracer ratio method (Tackley & King, 2003).

For this study, 25 models (see Table 1) with varying number of ACPs ( $0 \leq NC \leq 4$ ) and surface yield stresses ( $40 \text{ MPa} \leq YS \leq 150 \text{ MPa}$ , plus practically infinite in stagnant lid runs) have been computed. All cases are named accordingly, so a case without ACPs and with a surface yield stress of 40 MPa is named NC0-YS40. While the number of ACPs is varied, they always cover a total of 10% of the surface of a sphere, which is the approximate coverage of Venus' tessera regions (Ivanov & Basilevsky, 1993). However, our 2-D models only represent the equatorial slice of this 3-D sphere, and thus, the cylindrical ACP appears larger in this

geometry. The effectively applied angular radius of an ACP is given by  $r_{ACP} = \cos^{-1}(1 - 2A_{ACP})$ , where  $A_{ACP}$  is the fractional area of the ACP (here always  $A_{ACP} = 10\% / NC$ ). We did so to facilitate comparison of 2-D and 3-D results. For the latter, we computed some corresponding cases on a Yin-Yang grid with a reduced resolution of  $64 \times 192 \times 64 \times 2$  and  $1.44 \times 10^8$  tracers ( $\sim 93$  per grid cell). This resolution is rather coarse but allowed us to make the computation with acceptable computational effort. These cases merely serve as a consistency check for our 2-D results, as it was not feasible to compute all models in 3-D.

### 2.3. Diagnostics

For our reproducible postprocessing, we use the automated diagnostics and visualization of *StagLab* (Crameri, 2017, 2018). We tracked the overturn events using surface mobility, which is the ratio of the plate-core root mean square (RMS) horizontal velocity and the asthenospheric RMS velocity. In a stagnant lid model, surface mobility is  $\sim 0$ , whereas in a mobile lid model, the surface mobility is typically  $\geq 1$ . For an episodic lid model, the surface mobility will alternate: When  $\geq 1$ , an overturn is occurring, when  $\sim 0$ , there is no overturn, but a stagnant-lid phase.

Crustal thickness and surface age are computed to get an insight into the crustal production and renewal of the surface, even when overturns are absent. Crustal thickness is initially zero but changes due to eruption of molten basaltic material onto the surface and due to delamination and convective erosion at the crustal base. The new material emplaced on the surface resets the age of the surface, which is defined here as the residence time of tracer particles in the uppermost layer of the numerical model grid. Tracers can reach/leave this layer by volcanic and tectonic processes. That is, they rise to the surface either upon the extraction of melt and subsequent emplacement of crust (volcanic eruption) or when a spreading center develops where new, young lithosphere is generated (tectonic resurfacing). Recycling happens either via subduction or when older material is buried by newly emplaced volcanic material. Using this, distributions of surface age can be extracted from our models by averaging the age of all tracer particles within each grid cell. Both mean crustal thickness and surface age through time are strongly affected by the presence of ACPs, because the ACPs will retain a higher surface age and lower crustal thickness. ACP regions are thus excluded from mean values of these diagnostics presented in section 3, whereas they are still considered in presentations of surface distributions where lateral variations are of interest.

## 3. Results

The cases examined in most detail contain ACPs and feature episodic overturn events, but we first discuss two cases without ACPs as reference, one stagnant lid case (NC0-YS $\infty$ ) and one episodic lid case (NC0-YS40).

### 3.1. Reference Cases

In the stagnant lid case (NC0-YS $\infty$ ), the extreme yield stress inhibits overturn events. Mean mantle temperature increases initially, as the heat balance of the system is dominated by internal heating, but after  $\sim 1.5$  Gyr heat loss and internal heating become balanced, and a (statistically) steady state is reached (Figure 1a). Initially, there is no melting and therefore no volcanic eruptions, but melting sets in once hot plume heads rising from the CMB reach shallower depth. Volcanic activity increases until it reaches a steady state and the rate of volcanism is constant (Figure 1b). At this point, the numbers of plumes and convection cells also reach an equilibrium; in this case three plumes are observed (Figures 2a–2c). Convection in the mantle has limited impact on surface motion in this case; surface velocities remain below 0.3 cm/year.

In the episodic reference case (NC0-YS40), stresses in the lithosphere frequently reach the yield stress and initiate overturn episodes (Figure 1c). This is expressed by high surface mobility, which typically peaks when a new downwelling initiates during an overturn period. The associated slabs sink rapidly through the mantle and drag the attached surface material with them. For the low yield stress used here, the overturn episodes are typically global, so that the entire surface is subducted by either one or by a series of slabs during a short time period. Three such episodes are observed, which initiate at 0.09, 1.16, and 2.54 Gyr and last for 0.37, 0.66, and 0.83 Gyr, respectively. In our model, overturn events typically initiate with a spreading center. The onset of spreading is closely followed by the onset of subduction, caused by compression in the crust, often in the opposite hemisphere. Following this, the surface velocity increases, and the material subducts into the lowermost mantle, where it starts to wrap around the CMB (see Figure S2). This may shift the

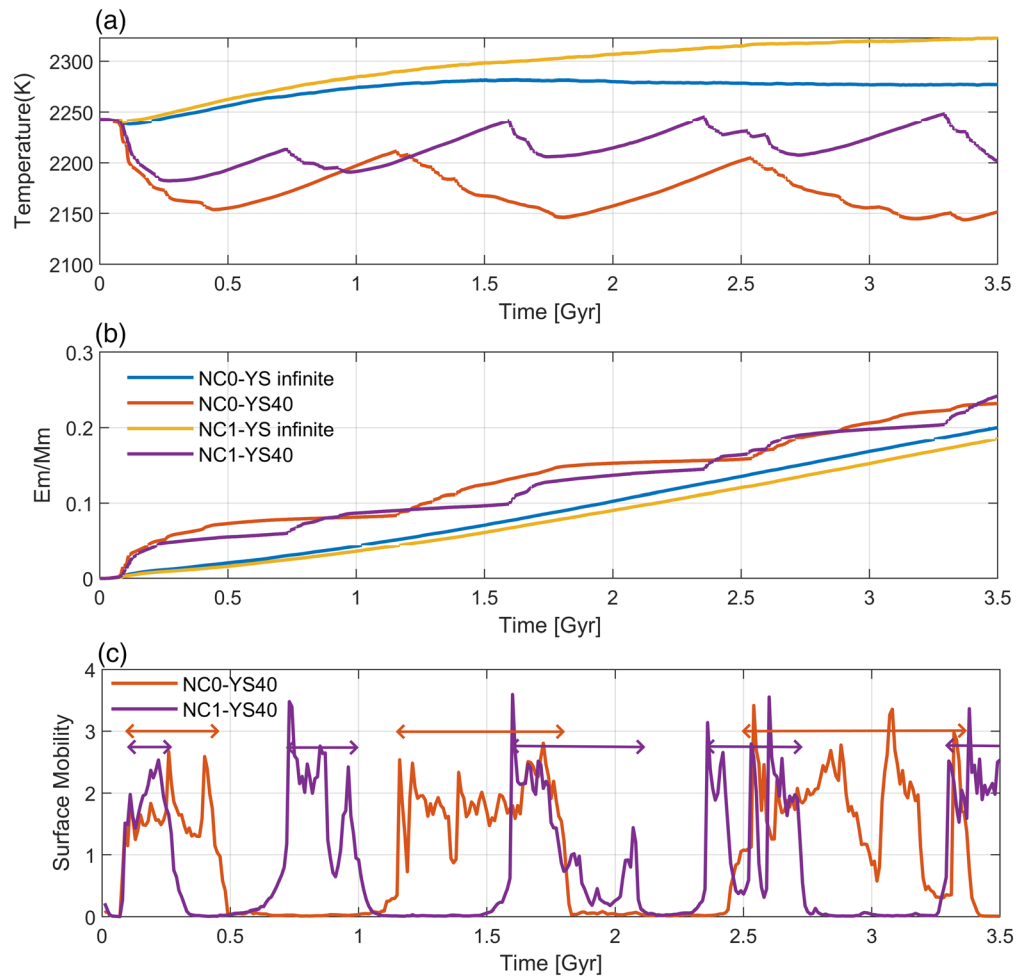


**Figure 1.** (a) Mean mantle temperature through time and (b) total mass of erupted material ( $E_m$ , cumulative) divided by the total mass of the mantle ( $M_m$ ); note that the slope of the curve is essentially the rate of volcanism and linked to the resurfacing rate. If  $E_m$  changes linearly within a certain time interval, then the rate of volcanism is constant over that interval. (c) Surface mobility for cases with  $YS = 40$  MPa; the durations of overturn events are marked by red and purple arrows.

center of mass away from the center of figure (King, 2018), which is in our model identical to the center of the spherical annulus. The compositionally anomalous layer can persist after overturn cessation, as remixing into the mantle is relatively slow (on the order of 0.5 Gyr). Upon remixing, the overlying mantle becomes less depleted in basaltic components again. When the entire slab is subducted, another subduction zone may initiate until the entire crust is recycled and the overturn episode ends. For cases with higher yield stresses than in this reference case, the overturn event may end after only a few subducted slabs, leaving sections of relatively old crust on the surface.

Recycling of cold surface material cools the mantle and causes a pronounced decrease in mean mantle temperature and the disruption of mantle plumes (Figure 1a). This reduces volcanic activity and resurfacing following the overturn for a while until the mantle has recovered its thermal state and overturn remnants have disappeared.

### 3.2. Effect of ACPs on Mantle Flow, Overturn Occurrence, and Frequency

#### 3.2.1. Differences in Flow Dynamics

Adding ACPs to the models changes the interior dynamics. Both stagnant and episodic cases containing ACPs yield higher mean mantle temperatures than the cases without ACPs. This is due to the insulating effect ACPs have on the mantle, as heat transport through the thick ACPs is inefficient. The mantle

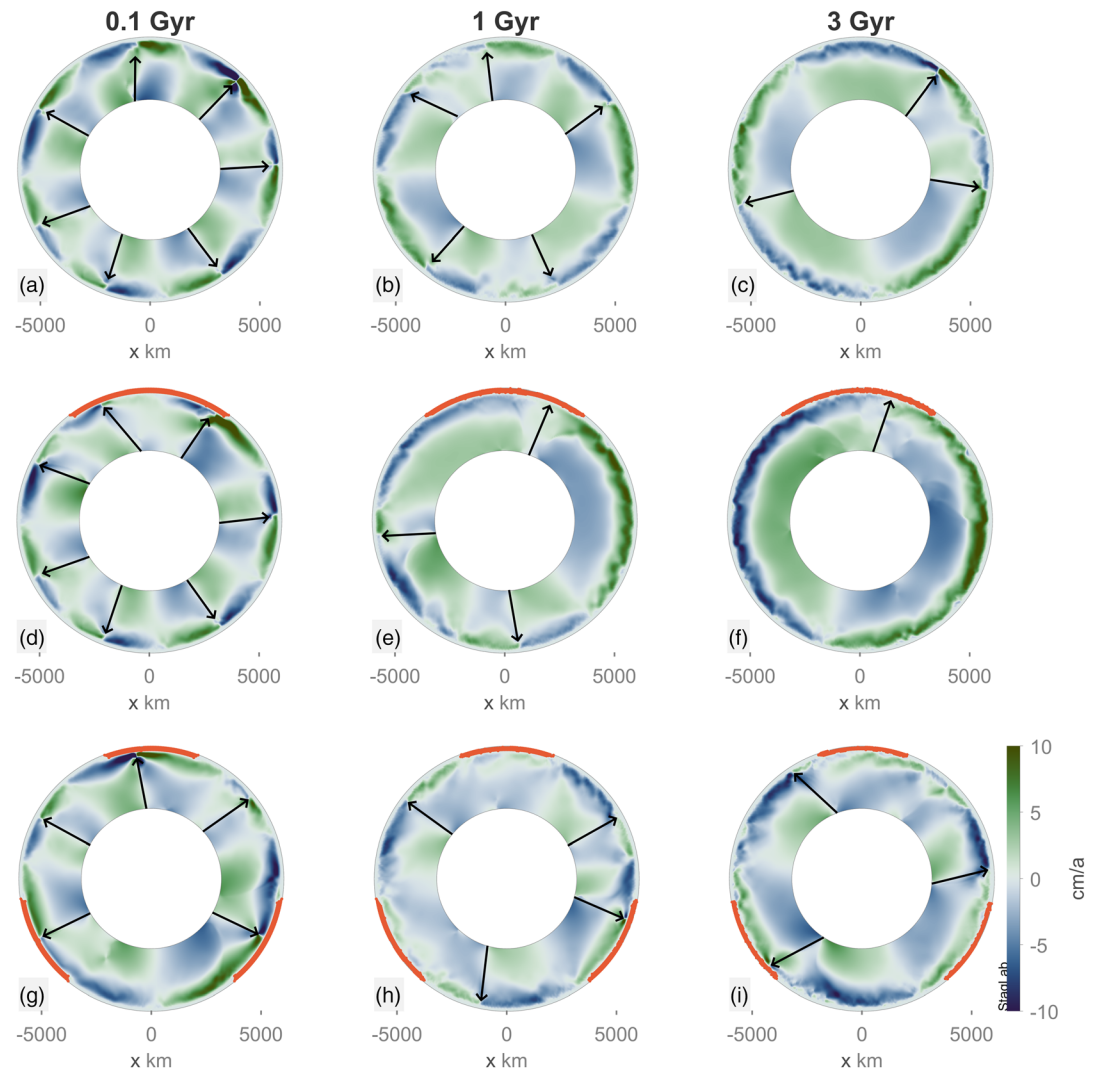


**Figure 2.** Horizontal velocity in the mantle, showing the decrease in number of convection cells in (a–c) NC0-YS $\infty$ , (d–f) NC1-YS $\infty$ , and (g–i) NC3-YS $\infty$ . Green areas indicate clockwise, and blue areas indicate anticlockwise motion. The black arrows denote upwelling plumes situated in the main areas of convergence in the flow field in the (deeper) mantle. The ACPs are indicated by the red sections on the surface.

temperature underneath the ACP is therefore slightly higher than the temperature in the remaining mantle (see Figure S3). For the stagnant lid cases, the mean mantle temperature for one large ACP is almost the same as for four smaller ACPs, whereas two and three ACPs yield lower mantle temperatures (see Figure S4). This trend is similar in the episodic cases, but more difficult to observe due to the rapidly changing temperatures caused by the overturn events. The differences in insulation of the mantle may be due to the way ACP sizes are implemented in our models. The sizes are determined from a 3-D sphere, where ACPs are placed on the equator. The 2-D model is essentially a cross section of this equatorial plane, so that an ACP that covers 10% of the surface of a 3-D sphere will cover less area in 2-D, than four ACPs covering 2.5% each. For a given total ACP coverage on a sphere,  $A_{ACP}^{tot}$ , the effective coverage on the 2-D cross section is given by  $A_{ACP}^{eff} = NC \cos^{-1}(1 - 2A_{ACP}^{tot}/NC)$  and is thus lower for  $NC = 1$  than for  $NC = 4$ . This suggests more insulation with more ACPs. On the other hand, thermal insulation is more efficient with a single larger rather than with multiple small insulating units, and the net effect of these two counteracting aspects may explain why the thermal response of adding ACPs in our model is not linear.

In addition to this thermal effect, the presence of ACPs changes the mantle flow pattern, the number of convection cells, and the positioning of plumes (Figures 2d–2f). One large ACP decreases the number of

convection cells from four to two and increases the dominant wavelength of mantle flow as previously indicated by numerical studies with terrestrial continents (see, e.g., Phillips & Coltice, 2010; Rolf et al., 2012) as well as in laboratory experiments of partially insulated convection (Guillou & Jaupart, 1995). The insulation underneath the ACP causes upward flow in this area, which is forced to the sides at the base of the ACP. Partial melting typically does not occur here because the relatively large ACP thickness imposed here (~230 km) leads to a thick thermal boundary layer, which prevents crossing of the solidus. As the ACP is rather large, the forcing of lateral flow below the ACP facilitates very long wavelength flow with only two convection cells (sometimes called “degree 1” convection). An ACP with half the size (5% coverage) produces a less distinct degree 1 pattern without clearly divided hemispheric convection cells (see Figure S5), and adding more ACPs clearly increases the number of convection cells (Figures 2g–2i). The surface velocity is not strongly affected by the addition of an ACP in the stagnant lid regime and stays small.

In episodic cases, overturns generally happen in a similar manner with and without ACPs present. The event initiates with a spreading center in one hemisphere and a subduction zone in the opposite hemisphere. With an ACP present, the spreading center is typically initiated in the vicinity of the ACP margin. The upwelling underneath the ACP causes the initiation to happen close to the ACP, but not exactly at the margin, possibly due to the lateral movement of material caused by the large size of the ACP. The initiation of spreading by the upwelling causes a state of compression in the opposite hemisphere, which finally results in a subduction zone. The ACP moves toward the subduction zone, and the overturn typically ends as soon as the ACP overrides the subduction zone. As the ACPs are strong, they generally do not participate in recycling and remain intact on the surface, although in some cases (NC2-YS80 and NC2-YS100), a small density difference ( $-20 \text{ kg/m}^3$ ) was assigned to the ACP root to make them more resistant to subduction.

A robust reason for why subduction typically occurs in the opposite hemisphere could not be established. However, higher lithospheric strength is known to promote longer wavelength mantle flow and thus a larger spacing between ridges and subduction trenches (e.g., Yoshida, 2008). The lithospheric strength here is very high, as the yield stress is not far from the transition threshold to a continuous stagnant lid (otherwise, continuous mobile lid behavior should be observed). This may explain the maximum, hemispheric-scale spacing of ridges and trenches with a single large ACP. With  $NC = 2-4$ , in contrast, convective wavelength is typically smaller, and the separation of divergent and convergent zones is less pronounced. When two ACPs move toward the same subduction and all material between them is subducted, they collide and stick together behaving as one ACP for the remaining model time as not enough tensional stress is generated to pull them apart again.

### 3.2.2. Condition for Overturn Initiation

Decreasing the yield stress is known to change the convective regime from stagnant lid to episodic lid and further to mobile lid, also in the presence of ACPs (Rolf & Tackley, 2011). With  $NC = 0$ , the transition between stagnant and episodic lid is observed at  $YS \sim 100 \text{ MPa}$  (Table 1). For cases NC0-YS40, NC0-YS80, and NC0-YS100 the first overturn is initiated at 1.15, 1.53, and 2.54 Gyr, respectively, indicating that initiation is delayed at higher yield stresses. The interval between different events remains similar; however, the duration of individual overturns is longer for  $YS = 40 \text{ MPa}$  (0.5–0.75 Gyr) than for  $YS = 80-100 \text{ MPa}$  (0.05–0.1 Gyr), which might be due to the overturns being global for  $YS = 40 \text{ MPa}$  and more local for  $YS = 80-100 \text{ MPa}$ .

The transition between stagnant and episodic lid also depends on the addition of ACPs. While the transition lies at 100 MPa with  $NC = 0$ , it increases when one and decreases when several ACPs are added (Table 1). The absolute differences in critical yield stress in our models should not be overinterpreted, but this trend may relate to the insulation of the ACPs and their effect on the flow pattern. One large ACP favors a two-cell convection pattern with one upwelling and one downwelling in opposite hemispheres (Figure 2f), as well as a more focused thermal insulation underneath the ACP. A higher number of ACPs favors flow patterns with a scale similar to those without ACPs (or even shorter; Figure 2i) and leads to more distributed thermal insulation, both of which can affect the distribution of generated stresses.

Addition of ACPs only alters the frequency of overturns in the lowest yield stress tested here (40 MPa). At this yield stress, all overturns are close to global, so that without ACPs the entire surface must subduct in order for the overturn to cease. When ACPs are present, there is generally less surface material to subduct, and the overturns thereby last shorter (Table 1). The NC4-YS40 case has seven overturn episodes; this high

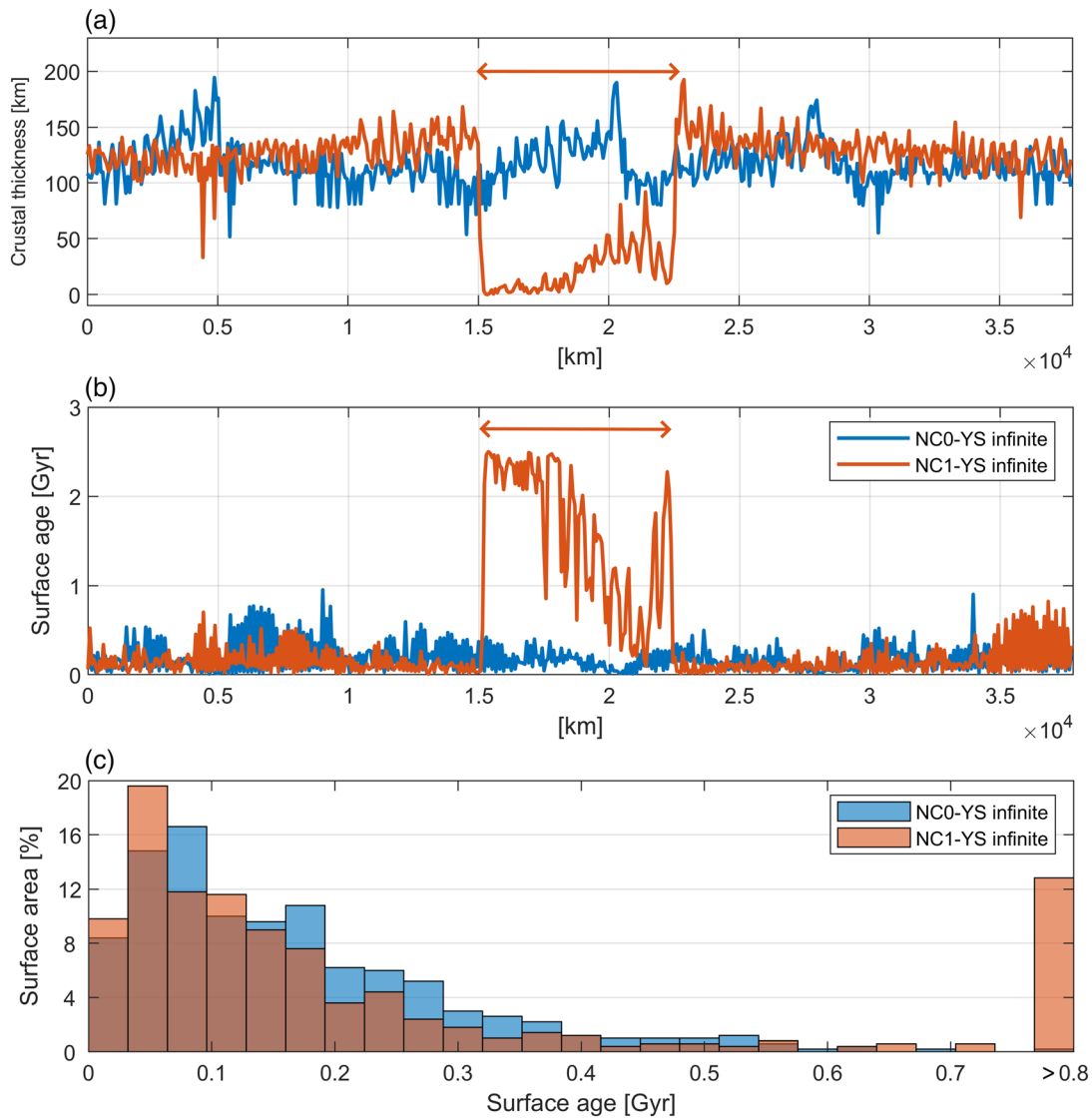


**Figure 3.** (a) Crustal thickness at 2.5 Gyr, showing the thinner crust on the ACP. The orange arrow indicates the ACP. (b) Surface age at 2.5 Gyr, showing the older surface on the ACP. The orange arrow indicates the ACP. (c) Surface age distribution for stagnant lid for  $NC = 0$  and  $NC = 1$  cases at 3.5 Gyr, with all surfaces older than 0.8 Gyr collected in the last bin, which mostly, but not exclusively, involves the contribution of the ACP.

number may be connected to the relative proximity of the equally distributed ACPs and the subduction zones. An overturn episode in this case is defined as a period of time where several slabs are subducted in quick succession. When the ACP starts moving, it will quickly override the subduction zone and shut it off. Another slab will initiate if there is still sufficient stress in the lithosphere and will subduct the remaining.

### 3.3. Survival of Crust Following an Overturn Event

Eruptions produce crust on the surface, but due to the thick thermal boundary layer at the ACPs, eruptions are less frequent here, and little crustal material is emplaced on top of them, leaving them with thinner crust and older surface than the remaining parts (Figure 3).

The surface away from the ACP is renewed more efficiently through eruptions and overturn events; the crust is thicker and generally younger than 1 Gyr (Figure 3c). In stagnant lid, mean crustal thickness away from the ACPs seems to be independent of added ACPs and follow the same evolution as cases without ACPs. Once an equilibrium between crustal production (via volcanic eruptions) and crustal destruction (via

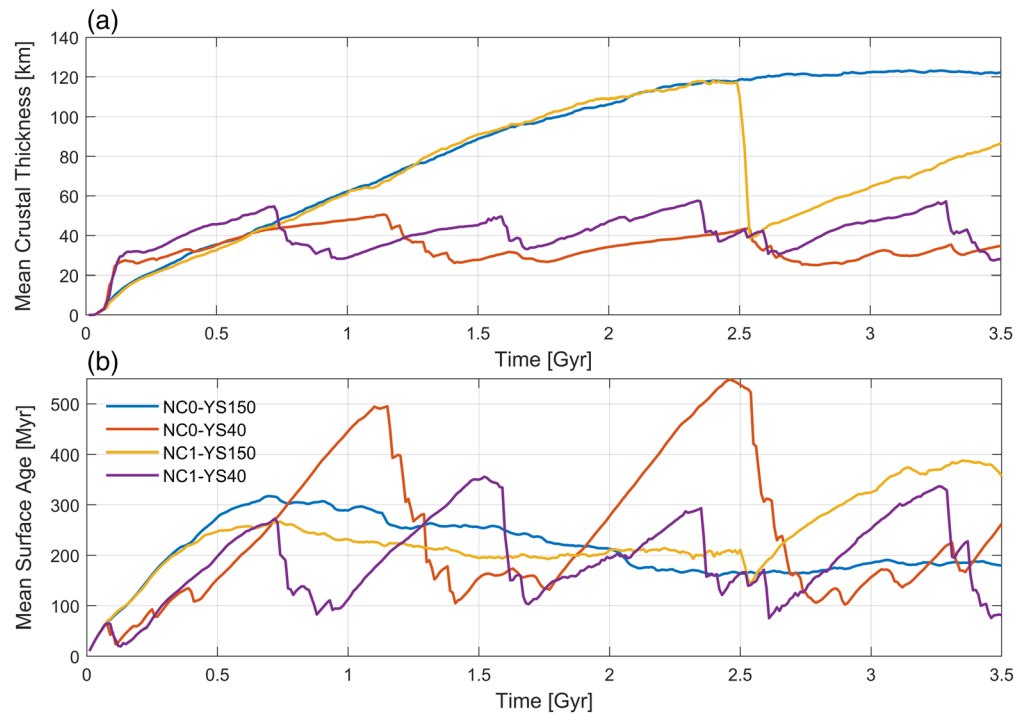


**Figure 4.** (a) Mean crustal thickness through time (ACP material is excluded from the mean) for models with varying surface yield stresses. (b) The same as (a) but for mean surface age through time.

dripping and convective erosion at the crustal base) is reached (here at  $\sim 2.5$  Gyr; Figure 4a), the basaltic crust has a large mean thickness of  $\sim 120$  km. At this point, mean surface age has a stable value of  $\sim 200$  Myr (Figure 4b), because resurfacing due to volcanic processes adopts a constant rate (Figure 1b).

Whenever an overturn takes place, parts of the crust are dragged down into the mantle, and new crust is produced at the spreading center, decreasing both crustal thickness and surface age drastically. Crustal thickness begins to increase again when the subduction ends but remains lower than that of the stagnant lid cases (Figure 4a). Surface age on the other hand increases further than in the reference case after the overturn events (Figure 4b). The deeply recycled crust disrupts the plume activity in the lower mantle and decreases the mean mantle temperature, which reduces for a while the rate of volcanism at the surface. As the plume pattern needs time to reorganize after an overturn event, in cases as much as 0.5 Gyr, this ultimately leads to greater mean surface age.

Without ACPs but with high yield stress ( $NC = 0$  and  $YS = 80\text{--}100$  MPa), parts of the lithosphere typically survive the overturn events. These parts can be up to  $\sim 1/3$  of the surface and are characterized by retaining a thick crustal root after the overturn event ended (Figure 5). In some cases, this is not visible in the surface age diagnostic, which may be globally reset during overturn, owing to a thin layer of young crust covering the surviving surfaces, in particular when they are small. Another way to define the age of material is to use the time since the material was last molten (Noack et al., 2012). This diagnostic has the advantage of being defined at all depth and not only at the surface. On the other hand, it only considers volcanic (eruptions) and not tectonic recycling (overturns), but due to the strong volcanic activity during overturns, this difference appears to be secondary. Analyzing this alternative age diagnostic reveals thick crustal roots feature ages that date them prior to the onset of the overturn (see Figure S6). Combining crustal thickness and age since last melted is the most robust diagnostic to detect portions of the lithosphere surviving overturns, but for simplicity we will base our subsequent discussion mostly on crustal thickness.

In case NC0-YS100, the overturn event at 2.5 Gyr exhibits two subducting slabs following each other closely in time. Each slab subducts  $\sim 1/3$  of the surface, which leaves the remaining  $1/3$  behind on the surface (Figure 5). At the initiation of the next overturn, however, this section is the first one to subduct due to its greater thickness and age.

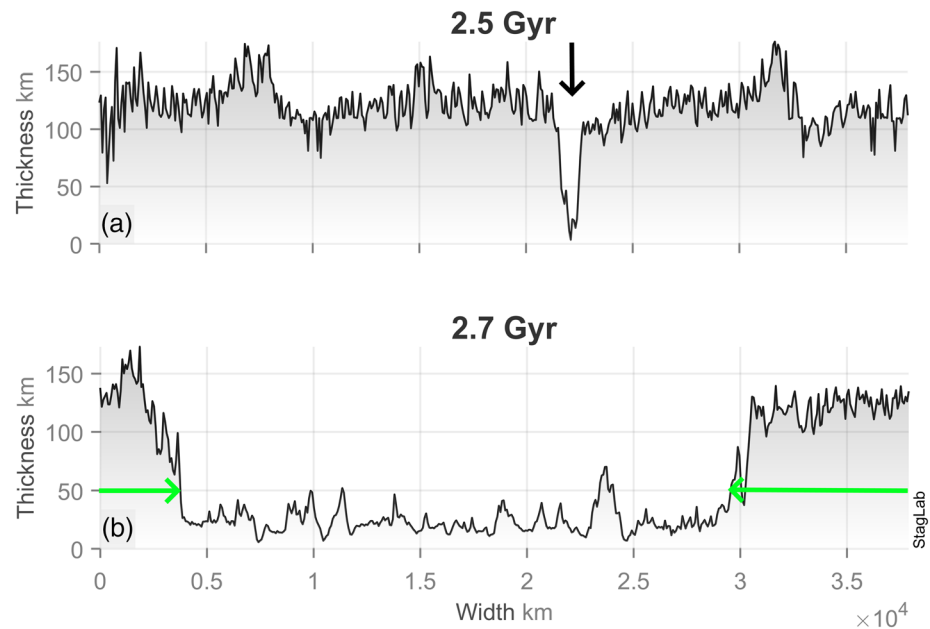


**Figure 5.** Crustal thickness (a) before and (b) after an overturn event for model NC0-YS100, the  $x$  axis shows the horizontal distance across the surface. The arrow in (a) indicates a spreading center, and the green lines in (b) shows the surviving, nonrecycled section covering  $\sim 30\%$  of the surface.

In contrast to this scenario, observed for rather high yield stress ( $YS = 80\text{--}100$  MPa), overturns appear more global with lower yield stress ( $YS = 40$  MPa), meaning that no parts of the lithosphere retain thickness and/or age after the overturn ended. In this case, the overturn consists of several slabs that follow each other in time and renew the entire surface during one overturn event. Thus, the behavior starts to resemble a mobile lid regime, in which distinct overturn events are not defined any more, but the surface is efficiently recycled and typically young.

When ACPs are present, nearly the entire non-ACP surface subducts during the close-to-global overturn events. While the ACPs resist overturn due to the chosen material parameters, there are also non-ACP surface portions, which survive the recycling event, seemingly just because an ACP is present (Figures 6–8). These parts are generally connected to an ACP, but not exclusively, and thus could be more appropriate analogs for Venusian tessera units. In case NC0-YS150, the surface material in between the ACP and the spreading center moves toward the subduction zone in the opposite hemisphere connected to the trailing margin of the ACP and thus never reaches the subduction zone: The strong ACP “shields” the weaker material at its trailing end from recycling (Figures 6 and 7). Depending on the placement of the subduction zone and the spreading center, another section of non-ACP crust can survive the overturn, if subduction cessation by the overriding ACP happens before the entirety of surface material on the opposite side of the spreading center has subducted (Figure 6).

In case NC2-YS80 with two ACPs, the survival of lithosphere differs a little from case NC1-YS150. The spreading center initiates in the area where the ACPs are closest to each other and the non-ACP section is split into two parts that move in opposite directions connected to a different ACP (Figure 8a). The subduction zone is located in the opposite hemisphere and as the ACPs move toward it, both shielded sections are split again by two new spreading centers (Figure 8b), which causes two detached non-ACP sections to survive, in addition to the sections still attached to the ACPs’ trailing edges. This behavior could be an expression of the more complex flow structure with shorter wavelength components when multiple ACPs are present (Figure 2).

Detecting surviving non-ACP surface after the overturn based on the surface age diagnostics is difficult, because of the thin omnipresent layer of fresh crust as described above. Still, it can be detected by examining the crustal thickness in cases where the crust has built up a certain thickness before the first overturn event,

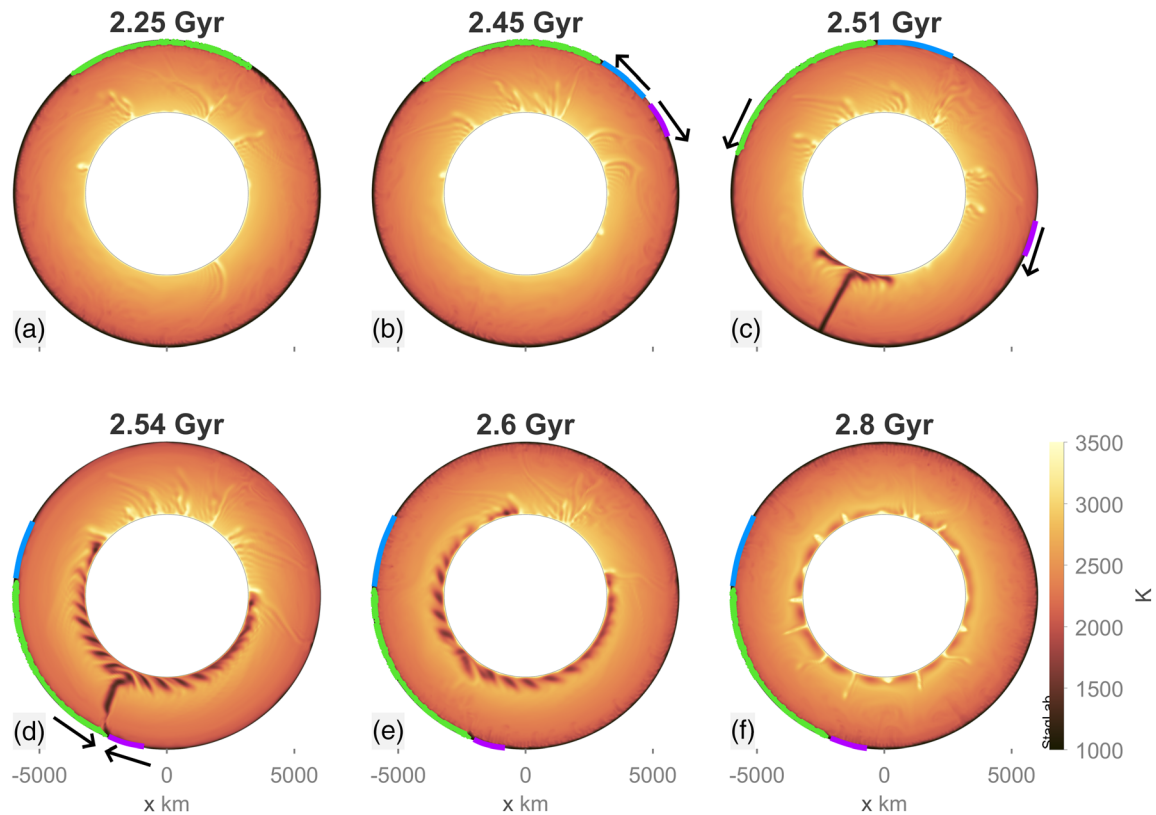


**Figure 6.** Evolution of an overturn in case NC1-YS150 showing the survival of two sections of non-ACP crust. The color scale shows the temperature. The ACP is marked by the green line, the overturn-surviving non-ACP section connected to the ACP is marked with blue, and the overturn-surviving non-ACP section on the opposite side of the spreading center is marked with purple. The black arrows mark the spreading center and the qualitative movement of the crust.

like in case NC1-YS150, where the first overturn happens late in the evolution (Figures 6a–6c). With frequent overturns (at lower yield stress), however, the detection is more difficult due to the generally thin crust before the overturn initiates. This is the case with  $NC > 2$  in our model suite as overturns only occur in this regime (Table 1). Independent of that, the survival of non-ACP crust is additionally complicated in our models with  $NC > 2$ , because the effective ACP surface coverage is increased and less non-ACP surface is present per se, but also because the ACPs typically collide during the evolution and squeeze out any non-ACP material in between them. However, our model suite contains only two episodic cases with  $NC \geq 3$ , which makes the described behavior difficult to generalize at this point.

Overturn survival is typically easier for the shielded surface section connected to the trailing margin of the ACP. The survival of sections detached from the ACP margin (as in case NC2-YS80; Figure 8) is only rarely observed (in two cases with  $NC = 2$ ) and seems to require a specific placement of the subduction relative to the spreading center(s). Since our setup is limited to symmetrical subduction, both converging plates have a similar velocity, so that the time required to reach the subduction zone is mostly given by the distance to the subduction zone. With more realistic one-sided subduction (Cramer et al., 2012), surface velocities will likely be more asymmetric, and this is expected to affect how overriding ACPs interact with an ongoing subduction system and also in which situations non-ACP surface that is detached from a shielding ACP may survive an overturn episode.

### 3.3.1. Comparison to 3-D

To test whether our findings from 2-D spherical annulus geometry are not fundamentally altered when adopting to a more realistic 3-D spherical geometry, we also ran three 3-D cases with the same setup as the corresponding 2-D cases. For computational feasibility, the horizontal resolution of the model had to be reduced (section 2). The qualitative evolutionary tendencies are similar in 2-D and 3-D, but some quantitative differences are apparent. For instance, mean mantle temperature (by  $\sim 70$  K) and crustal thickness

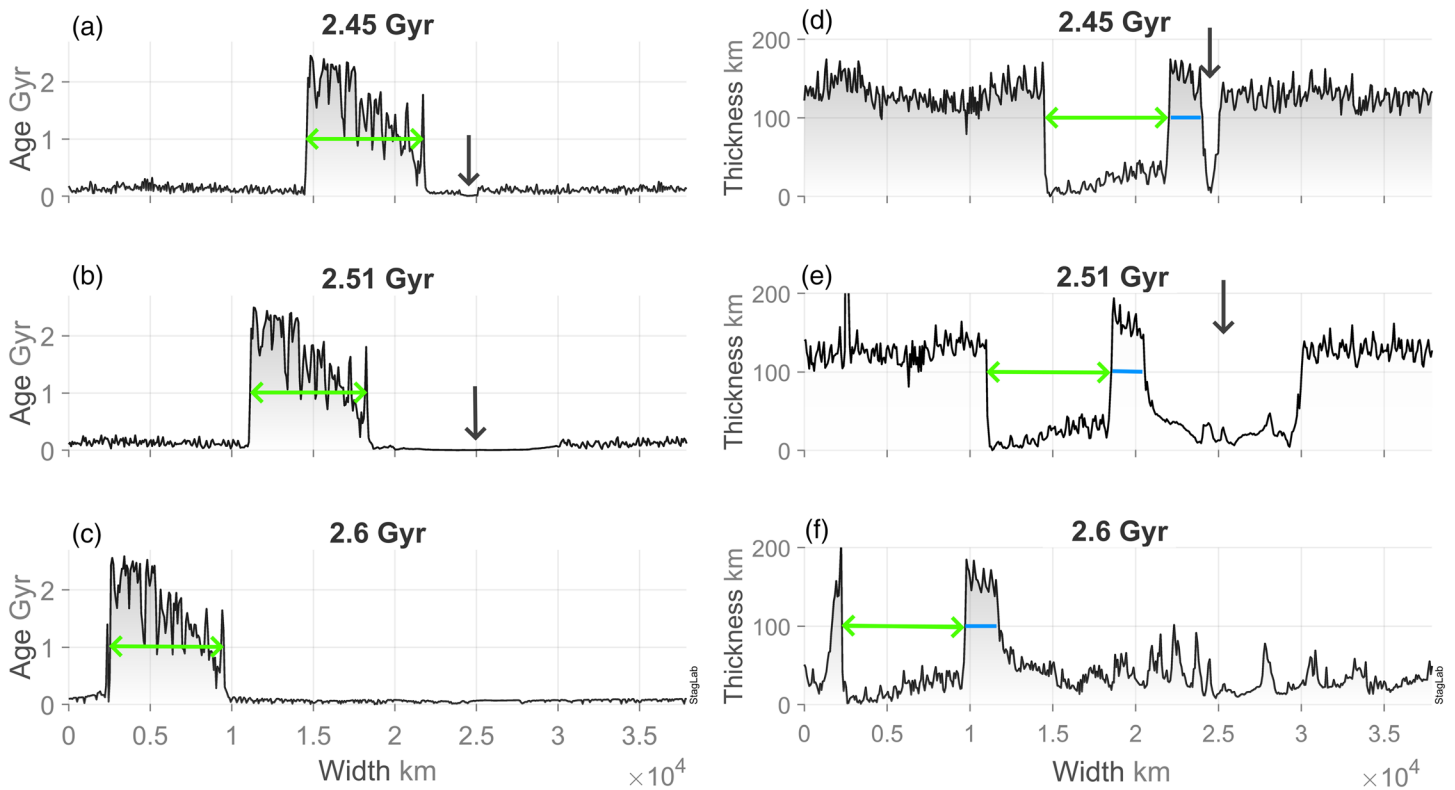


**Figure 7.** (a–c) Surface age and (d–f) crustal thickness for the same case as in Figure 6 (NC1-YS150); the  $x$  axis shows the horizontal distance across the surface. The ACP is marked by the green line, the surviving section connected to the ACP is marked in blue, and the surviving section on the opposite side of the spreading is marked in purple; the spreading center is marked by vertical black arrows.

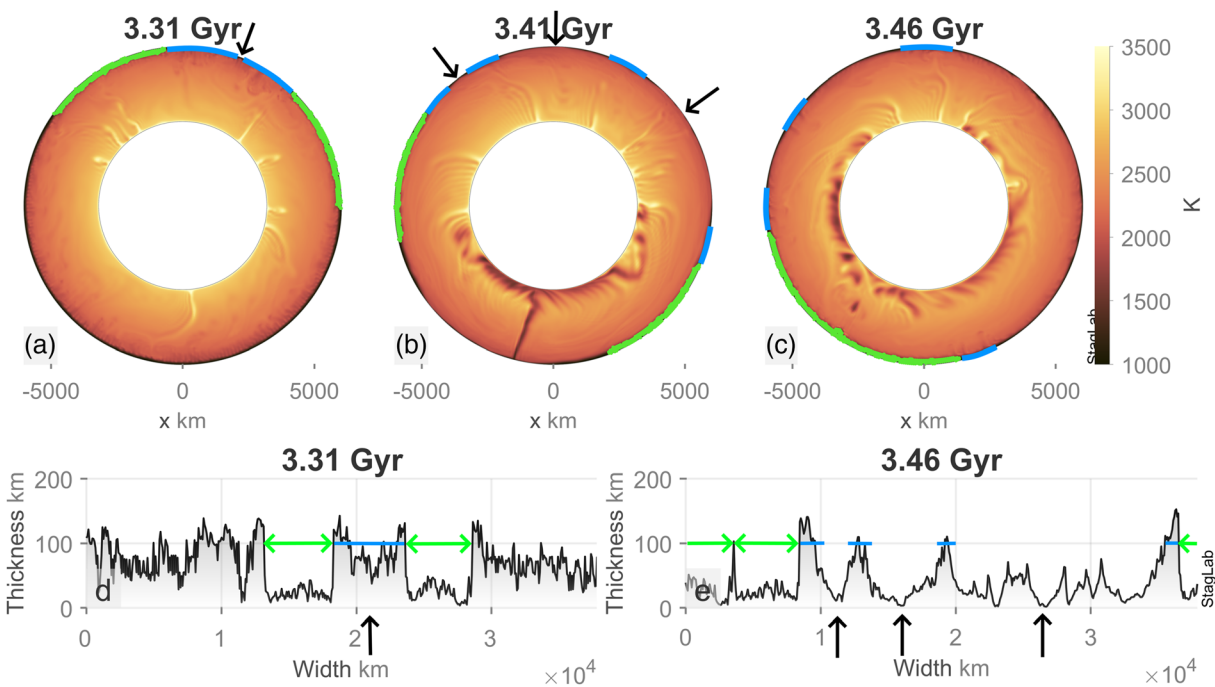


**Figure 8.** (a–c) Evolution of an overturn event in case NC2-YS80. ACPs are marked by the green lines, surviving sections are marked by blue lines, and spreading centers are marked by black arrows. (d and e) Crustal thickness of the first and last time steps, corresponding to panels (a) and (c), respectively; the  $x$  axis shows the horizontal distance across the surface, and the black arrows mark the spreading centers.

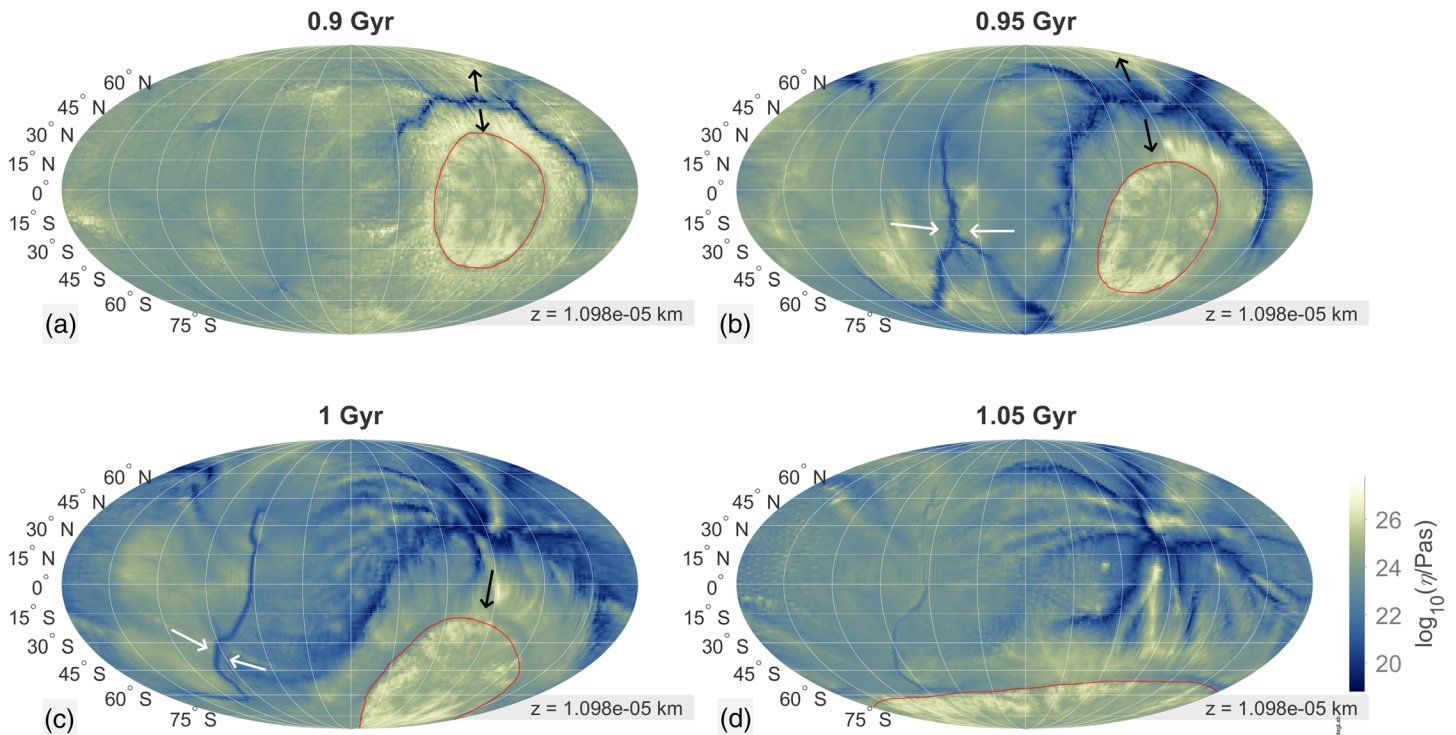


**Figure 9.** Mollweide projections of viscosity at depth  $z$  below the surface in a 3-D case with  $NC = 1$  and  $YS = 80$  MPa, which display the evolution of an overturn event. Black arrows mark spreading centers, and white arrows mark subduction zones; the ACP is marked by a red contour.

(by  $\sim 20$  km; Figure S7) are somewhat lower in 3-D, possibly due to different flow topologies (e.g., Guerrero et al., 2018). For instance, upwellings are columnar features in 3-D with rather local effects, while they are sheet like in 2-D and have more impact on the globally averaged thermal state. If crustal production is linked to hot upwellings, this could explain why the global mean thickness of crust is different in both geometries. During overturn events, however, mean crustal thickness decreases to the same minimum value of  $\sim 40$  km in 2-D and 3-D (Figure S7).

As in 2-D, the presence of one ACP favors overturn initiation, whereas multiple ACPs ( $NC = 2$ ) seem to complicate it. When compared to our 2-D simulations, the 3-D cases tend to require a somewhat lower yield stress to adopt the same tectonic behavior, possibly because the extra dimension allows material to deform in a way that reduces the peak stresses generated by mantle flow. Although Guerrero et al. (2018) used a different model setup (e.g., no ACPs, no melting, no phase transitions, and no plasticity), we note that these authors also reported that 3-D spherical models can exhibit a different tectonic regime than 2-D annulus models employing the same physical parameters. In particular, they observed that 3-D models display the stagnant-lid regime for a smaller temperature dependence of viscosity than 2-D models, which effectively determines the relative strength of the lithosphere (if plastic yielding is not considered). In other words, a stagnant lid may form at lower lithospheric strength in 3-D, which would match our observation that a lower yield stress is needed in 3-D to adopt the 2-D behavior.

Overturns in 3-D also initiate with a spreading center located close to the ACP margin, similar to the 2-D cases. In case  $NC1$ - $YS80$ -3D the ACP moves toward a subduction zone located on the western side of the ACP (Figures 9b and 9c). Similarly, a section of non-ACP crust attached to the trailing ACP margin seems to survive the resurfacing and retains its crustal thickness after the overturn has ended (Figures S8–S9). Surviving sections detached from the ACP are not detected in the 3-D cases, but we could analyze only a very small number of 3-D cases. Interestingly, the overturn event is close to global, even though the ACP only moves by  $\sim 90^\circ$  toward the South Pole. Here, it interacts with the convergent zone where surface is recycled, but compared to the 2-D setup, the ACP cannot shut down subduction across its full length so easily. The recycling can thus continue in different locations on the globe, which may explain the close-to-global resurfacing.

For a case with  $NC = 2$  in 3-D, the spreading zone initiates close to both the ACPs, and they are dragged toward the subduction zone. The overturn is not effective enough to be global (e.g., due to the 2-D and 3-D discrepancy outlined above) and ceases without the ACP overriding the subduction zone, similar to what occurs in 2-D models with  $NC = 0$  and  $YS = 40\text{--}80$  MPa, meaning that both the section of crust closest to the ACPs and another section of the crust survive. This is different from the 2-D models with  $NC = 2$  where the overturn is global and only sections connected to an ACP survives.

## 4. Discussion

Our modeling provides instructive insight into the link of mantle convection and resurfacing, the effects of ACPs during surface-overturn events, and potential lithosphere survival. As with any modeling study, it is crucial to consider these insights in the light of the modeling limitations. We therefore discuss all these aspects in the following sections.

### 4.1. Crustal Thickness and Surface Age

The model predicted crustal thickness (away from ACPs) in the stagnant lid regime typically reaches values of  $\sim 100\text{--}120$  km in both 2-D and 3-D geometry (Figures 4 and S7). In comparison to the terrestrial setting with active plate tectonics, this value appears extremely large. In that setting, eclogitization would likely make the crustal base prone to delamination (e.g., Johnson et al., 2014). We argue that the delamination process is limited, because the 120 km thick crust is still thinner than the thermal boundary layer in our models. The thickness of the cold (and thus highly viscous) boundary layer controls crustal growth, as any excess crust would be eroded from below.

This suggests a reduction of mean crustal thickness in more vigorous mantle flow (i.e., reduced mantle viscosity) with a thinner boundary layer. This has been reported by Rolf et al. (2018), but the trend appeared relatively weak and would require an unreasonably low upper mantle viscosity to reduce crustal thickness to only several tens of kilometers, as it is inferred from other independent estimates (e.g., James et al., 2013; Wei et al., 2014). This would not align with Venus' upper mantle viscosity constraints from gravity and topography observations (Rolf et al., 2018; Steinberger et al., 2010). A thinner crustal layer in the stagnant lid regime may still be possible, though, in particular by considering crustal intrusions (Lourenço et al., 2018, 2020) and/or by using a stronger temperature dependence of viscosity (larger activation energy); we could not employ either of these measures because of numerical feasibility. In contrast, the episodic lid models generate crustal thicknesses in the range of 20–120 km depending on the frequency of overturns and especially the time passed since the latest overturn (Figure 4). Cases with frequent overturns (i.e., with low yield stress) generally have crustal thicknesses of 20–60 km. These values seem to fit better with previously estimated crustal thicknesses from modeling and observational data (Anderson & Smrekar, 2006; James et al., 2013), although still at the upper end.

Predicted mean surface ages for stagnant lid cases are generally below 300 Myr, whereas the episodic cases feature older surfaces. While only two of our models generate mean surface ages above 500 Myr (cases NC0-YS40, Figure 4b, and NC2-YS80), the episodic cases again lead to a seemingly better match with estimates for Venus, like  $750^{+350}_{-400}$  Myr (McKinnon et al., 1997). In contrast, younger mean ages have been postulated, and analysis of VIRTIS emissivity data indicates recent volcanic activity and resurfacing on Venus, although with relatively small volume, which points to a regime of (slower) equilibrium rather than catastrophic (overturn) resurfacing. Specifically, Smrekar et al. (2010) suggest recent volcanic flows with volumes of  $2,500\text{--}25,000$  km<sup>3</sup> perhaps as young as 2,500–25,000 years, which implies volcanic eruption rates in the range of  $10^{-1}\text{--}10^1$  km<sup>3</sup>/year. As a comparison, our 3-D stagnant lid model (3D-NC2-YS80) predicts a much larger volcanic eruption rate of  $\sim 56 \pm 4$  km<sup>3</sup>/year. Case 3D-NC1-YS80 (Figure 9) with several overturn periods indicates similar rates before the onset of overturns. During overturns, eruption rate doubles ( $>120$  km<sup>3</sup>/year), but after cessation it is typically reduced for some time, which explains why episodic cases can generate a globally older surface. Even during these periods, however, the rate remains as large as  $\sim 30\text{--}40$  km<sup>3</sup>/year, which would emplace a global equivalent layer of 1 (10) km thickness within  $\sim 15$  (150) Myr. The fact that we still observe clearly larger mean surface age than this is probably an expression of the nonhomogeneous distribution of volcanism, which is more pronounced above hotter mantle regions. In any case, such exaggerated large volumes of volcanic eruption indicate the limitations of our model. If

we assumed a 1:10 ratio of extrusive and intrusive magmatism as some terrestrial studies suggest, predicted eruption rates may reduce to  $\sim 3 \text{ km}^3/\text{year}$  or perhaps less by additionally considering preferred partitioning of heat-producing elements into the melt and eventually the crust.

Even though the currently predicted rates are exaggerated and the underlying model should be improved in the future, they still provide an interesting perspective, namely, that Venus' resurfacing history may be in a hybrid mode in which large-scale tectonic overturns can occur but are separated by extended phases of tectonic quiescence in which the planet adopts a largely volcanic, equilibrium style of resurfacing. How the two modes alternate or coexist during the evolution of the planet and shape its present crustal characteristics remains unclear though and is probably highly dependent on the model setup. Armann and Tackley (2012) carried out thermochemical modeling of Venus' mantle in 2-D, and their best fitting results favor frequent overturns, whereas Rolf et al. (2018) favors fewer overturn events in their 3-D models.

ACPs are implemented in our models as essentially rigid units and cannot yield; therefore, they are not recycled by overturn events and have crustal thicknesses and surface ages that are vastly different from the remaining surfaces. The crustal thickness is lower, because the large ACP thickness inhibits eruptions. Consequently, surface age is higher due to the low rate of resurfacing. In this regard, we emphasize that ACP thickness is merely imposed in our model. Venus does feature large plateaus, such as Ishtar or Aphrodite Terra, with high topography and comparably thick crust (James et al., 2013; Wei et al., 2014), but thickness estimates do not exceed 50–70 km. While these are modeling outcomes rather than direct observables, our imposed ACP thickness of  $\sim 230 \text{ km}$ , which was taken in analogy to that of terrestrial cratonic roots, is likely exaggerated. We computed an additional stagnant lid model in which ACP thickness was only half the nominal value. This thinned the boundary layer at ACP locations and facilitates eruption on top of the ACP and made their surface age more comparable to surrounding regions. But the growing crustal load pushed ACP material downward into the mantle and caused it to detach from the bottom and finally get recycled into the mantle (Figure S10). In our test with  $NC = 1$  and  $YS = \infty$ , the ACP ultimately dissolved despite its high strength, and only a part ( $\sim 50\%$ ) remained intact at the surface. We have not tested reduced ACP thickness in the episodic regime, but this initial test suggests that it is an important parameter to test in future.

The density of ACP material is also relevant and may be expected anomalous if the ACPs differ compositionally from surrounding regions. In this study, we achieved the long-term stability of ACPs by imposing higher yield strength and viscosity. Reducing density was (mostly) not needed to ensure stability; however, this would impact the build-up of ACP topography. Satellite measurements suggest that  $\sim 80\%$  of Venus' surface has relatively low topography ( $< 2 \text{ km}$  above the mean planetary radius; e.g., Hansen, 2018) and the remaining 20% accounts for highland regions, such as Ishtar Terra. We estimated model-predicted topography from the normal stresses at the surface. Without ACPs, the predicted topography range is mostly within  $[-1, 1] \text{ km}$  and thus broadly representative of Venus' lowland and mesoland (Hansen, 2018), but no large-scale highlands were observed. During overturn episodes, the predicted range is typically broader, especially due to up to 5 km deep trenches forming at the major recycling sites, which are not seen on present' Venus, but pronounced highland regions are still not observed. Since we do not assign a density contrast to the ACP, it adopts the reference density (see Table A1) and is thus effectively denser than the crust and the upper mantle phases of non-ACP material. The ACPs therefore correlate with topography lows in our model, which seems unrealistic compared to Venus' crustal highlands. Reducing their intrinsic density in future models should result in their uplift and a topography comparable to Venus' highlands, where also many (not all) of the planets' tesserae are hosted (see, e.g., Hansen, 2018).

Given the described limitations of our ACPs, their high surface age compared to their surroundings (Figure 3) should not be directly related to the potential age contrasts of Venus tesserae in comparison to other geological units of the planet. It seems unlikely that tesserae are several Gyr older than their surroundings as our model indicates. However, tesserae ages are estimated by crater counting, which assumes that the craters have remained intact since they formed. If tesserae have been subject to strong deformation instead, for example, during an overturn, some craters on them may be strongly degraded, which complicates their age estimate from crater density, and they may be older than they seem. The number of deformed craters on tesserae is small though, so if they were much older, then many craters must have been completely erased (Romeo & Turcotte, 2008). Such crater degradation and destruction processes are not considered in our model. One such mechanism is burial by lava flows, which is observed even on present-day Venus

(Shalygin et al., 2015). Such lateral flow of lava would in principle also affect the surface age and its lateral variations predicted by our model, but practically only if the size of Venus' lava flows exceeds the model's grid resolution. Some Venusian lava flows such as in Mylitta Fluctus (400–1,000 km; e.g., Roberts et al., 1992) may be large enough, but the global importance of this effect may be minor. In summary, it can be stated that tesserae age estimates from crater counting represent lower limits, while our model age estimates indicate upper limits. Improving the geological mapping and crater counting, on one hand, and our model, on the other hand, is required to achieve better convergence in the future. For now, the predicted ACP ages seem unlikely to represent the actual ages of Venus' tesserae, but our test with thinner ACPs, as described above, already shows a way to generate less extreme age contrasts.

#### 4.2. Effects of ACPs on Overturn Events and Survival of Lithosphere

The transition between stagnant and episodic lid regime in our models depends on the yield stress and to some extent on the presence of ACPs. Decreasing the yield stress facilitates initiation of overturns, and the yield stress at which the convective regime changes from stagnant to episodic lid is slightly different depending on the number of ACPs. With one ACP, the threshold yield stress between stagnant and episodic lid increases by <20 MPa (25%) compared to cases without ACPs. Adding several ACPs causes the threshold to decrease by <20 MPa for two ACPs and <60 MPa (60%) for three and four ACPs (Table 1). This shift in threshold yield stress might be due to the insulating effect ACPs can have on the mantle. On Earth, the partial insulation of continents decreases viscosity and thereby increases the velocities in the mantle and speeds up subduction, which increases heat loss from the mantle and causes cooling. These processes eventually link to the stress state in the lithosphere and thus overturn initiation. The effect is greatest for large continents and decreases with decreasing size (Lenardic et al., 2005) and is thus most relevant for our models with only one ACP.

Mean mantle temperature increases with added ACPs, but the relationship between the temperature increase and the number of ACPs is not linear (section 3.2.1) and can therefore not solely explain the shift in threshold yield stress. In fact, the mantle flow pattern appears to correlate better with this shift: One ACP promotes very large convection cells and a strong upwelling underneath the ACP (Figure 2). In contrast, more ACPs lead to more convection cells and several upwellings distributed across the mantle. This affects the stress distribution in the lithosphere: In our stagnant lid cases, for instance, we observe the highest surface stresses for  $NC = 1$  followed by  $NC = 0$ . For  $NC = 3$ , the surface stresses are shifted to somewhat lower values again, which reflects the trend in the transition stress as indicated in Table 1.

During overturn events without ACPs, large parts of the lithosphere subduct, but some sections resist recycling. The surviving fraction depends on the yield stress: at high yield stress (80–100 MPa in our model), as much as 1/3 of the lithosphere withstands recycling, because recycling typically happens through one or very few subduction zones, where only parts of the old and strong lithosphere are dragged along and recycled. At lower yield stress the surviving surface fraction is clearly smaller, because several smaller recycling events overlap and renew almost the entire surface. In this sense, the overall impact of the resurfacing events seems more global in the latter case, even though individual subduction zones are stronger at higher yield strength (closer toward the transition to permanent stagnant lid). As it is unlikely that tesserae have survived on the surface since the formation of the planet, the surviving sections in cases without ACPs could be a better representation of tessera regions than the preimposed ACPs. Their age contrasts are closer to that of the tesserae, as these might have formed only a short time before the remaining surface and survived the latest overturn event. The lateral distribution of surviving non-ACP material, on the other hand, is different as the tesserae are clustered in separate regions on Venus, whereas the modeled surviving crust is often only continuous section. This may be a limitation of our 2-D geometry, but we note that nonglobal, incomplete overturns were also reported from a 3-D spherical model with overturns by Weller and Kiefer (2019).

Adding ACPs prevents an overturn being global by definition, because the ACP is designed to resist these events. It is clear from terrestrial studies on continents, though, that this resistance strongly depends on the density and rheological properties of the ACPs. In particular without the assumed stronger rheology, ACPs would be destroyed during overturns (Lenardic et al., 2003). For cases with  $NC \geq 2$  we observe that the ACPs tend to collide when two ACPs move toward the same subduction zone and all material in between them is subducted. When these collisions occur, ACPs stick together throughout the remaining model time and continue to behave as one larger ACP because they are modeled in a way that makes them unable to yield. This is unlike what we observe for real continents on Earth, where collisions and breakup follow

each other in cycles (Buitert & Torsvik, 2014). The weak zones produced when continents collide are not implemented in this model, which strongly complicates breakup. In improved models with added weak zones at continental margins breakup of continental clusters seemed to be facilitated (Lenardic et al., 2003; Rolf et al., 2014; Yoshida, 2010), but though important for the evolution of Earth's continents, it is unknown whether this has any relevance for Venus' evolution since there is no evidence for any such behavior.

Besides this rather trivial preservation of ACP during surface mobilization, ACPs seem to enforce more global-scale resurfacing at high yield stress, because they increase the wavelength of mantle flow (Figure 2). That means ACPs have to move a larger distance to a subduction system in the opposite hemisphere before they can shut it down. Nevertheless, a small portion of lithosphere may survive resurfacing in this scenario as the ACP shields the lithosphere at its trailing margin from being subducted into the deeper interior. The sizes of the surviving sections are mainly independent of the number of ACPs and have a lateral extent of 2,000–4,000 km (4–8% of the surface area). The surviving section at the trailing end of the ACP generally reverts to the same crustal thickness as the remaining surface, by erosion from beneath, before the next overturn initiates. The new spreading zone may initiate in the same area as during the previous overturn, preserving approximately the same amount of non-ACP material. The effect of shielding non-ACP material from subduction may be more pronounced in 2-D geometry, but we observe similar shielding behavior in 3-D test cases (Figure 9). For lower yield stress (like  $YS = 40$  MPa), however, the lithosphere is relatively weak, which leads to global-scale resurfacing also without ACPs. In fact, in this scenario the presence of ACPs can even hamper global recycling, because subduction zones are typically weaker and located closer to the ACP margin, so that the ACPs must travel a shorter distance to reach the subduction zone and to possibly shut it down more easily than in the high yield stress situation.

#### 4.3. ACPs as Representatives of Venus' Plateau and Tessera Regions

After examining these effects of ACPs in our models and relating them to Venus, the modeled ACPs are likely to be an insufficient representation of tesserae regions. The tessera regions may not be as long-lived as the ACPs are in our models, although their actual age is difficult to constrain, due to their small size, which complicates crater statistics. However, the age of the model ACPs is enforced by the rather extreme rheological parameters and thickness we use to ensure their long-term stability. With more moderate physical properties, ACP material may be strong enough to resist one, but not several overturn events. A potential geological unit analog on Venus may still be found in the plateau units, some of which are surrounded by tessera units. Currently, Venus' tesserae ages seem closer to the mean planetary age than is the case for our ACPs. If this holds, tesserae might be better represented by the sections of (non-ACP) crust that survive overturn events in our models. Specifically, this happens in the high yield stress simulations ( $YS = 80$ – $100$  MPa). These areas form in between two overturn events but are not renewed by the overturn, thereby retaining a thicker crust than the remaining surface. The thickness assigned to the ACPs is probably also too large compared to the thickness of tessera regions. Thinner ACPs experience more frequent eruptions, leading to a younger ACP surface, but thinner ACPs have a tendency to get recycled. Reducing the density of ACP material may help to stabilize them and will also lead to a topographic signal that matches the typically elevated topography of tessera regions. Also, it may be more reasonable that rising magma forms intrusions within the ACPs rather than volcanic eruptions, which our model currently does not allow for. Surviving sections are also much larger in lateral size and usually restricted to one region, whereas the tesserae are smaller and scattered on the surface. In the 2-D geometry, however, it is difficult to relate the lateral placement and size of such sections to a realistic 3-D planet. In summary, further exploration of model parameters is needed to ultimately decide how well ACPs can represent Venus' tessera regions.

#### 4.4. Model Limitations

Our model includes to first order the interplay between flow in the mantle, mineral physics, rheology, and melting processes. Nevertheless, our model is strongly simplified compared to Venus, both in terms of implemented physical processes and in the applied parameter values (e.g., reduced activation energy and thus weaker temperature dependence of viscosity). Most of the simplifications have been discussed in the previous sections already; further points can be found in the study of Rolf et al. (2018). Generally, too little is known about Venus, so that we often use terrestrial analogs to specify properties. A striking example is that the ACPs are implemented in analogy to the Earth's cratons, which they are stable and largely resistant against deformation throughout the evolution. Ideally, ACPs would form self-consistently during the

evolution so that for instance their thickness would become self-organized, but this is beyond the scope of this work. The 2-D sizes of the implemented ACPs are based on a 3-D sphere causing the total covered area of the model to increase as more ACPs are added. If the effective coverage had been the same in 2-D, the effect of ACPs may decrease with increasing number of ACPs, but here, the effect increases with more ACPs because of higher effective coverage.

Recycling during overturns happens largely symmetrically in our Venus mode, while subduction on Earth is single sided. The efficiency and time scales of crustal recycling may differ in both modes. However, whether enforcing more Earth-like conditions with implementing single-sided subduction (Crameri et al., 2012; Gerya et al., 2008) also leads to a more realistic model for Venus is unclear. For instance, potential sites of previous subduction on Venus point to a somewhat different style of subduction than on Earth. Subduction on Venus may be less effective in pulling trailing plate portions and may be more dominantly induced by mantle plumes and a hot lithosphere, perhaps more comparable to early Earth (Davaille et al., 2017).

All magma in our models erupts as extrusive volcanism. This simplification strongly affects eruption rates, but also heat loss from the mantle as intrusive magmatism may thin the crust and ultimately cool the mantle, whereas extrusive volcanism thickens the crust and prevents efficient cooling (Lourenço et al., 2018). Thus, mantle temperatures may be lower than observed in our models. Intrusive magmatism also leads to a warmer and weaker lithosphere (Rozel et al., 2017), which could in turn facilitate overturn events or even promote a different tectonic regime (Lourenço et al., 2020).

## 5. Conclusions

Venus' tectonic regime remains debated, but an episodic regime with stagnant-lid periods interrupted by overturn events that recycle the surface efficiently is a possibility. Moreover, Venus' surface—generally rather uniform in age—features regions, the tesserae, which are older than the latest overturn events. This indicates the survival of parts of the surface during this event. The details of the overturn process, how it is triggered, how it ceases, and how it recycles the surface, remain only partly understood. Here, we use (mainly 2-D) numerical models to investigate this. Specifically, we impose a number of ACPs and investigate how they affect the interior evolution of a Venus-like planet in the stagnant and episodic lid regime. ACPs are implemented as preexisting, thick, and compositionally distinct provinces, which could relate to some of the large, continent-sized crustal provinces inferred for Venus. We examine the thermal state of the interior during stagnant lid phases and episodic overturn events, derive crustal thickness and surface age diagnostics, and investigate how ACPs affect overturn dynamics. Our main findings are as follows:

1. In stagnant lid, thick ACPs lead to slightly increased mantle temperature due to thermal insulation and enforce, for large ACPs in particular, a longer-wavelength flow pattern with less convection cells and plumes. Thinner ACPs induce weaker effects and may be less stable against recycling on long time scales.
2. Thick ACPs have moderate impact on the initiation of episodic overturns depending on their size and lateral extent. A single, large ACPs may facilitate overturn, but multiple small ones may complicate it, as the effects on thermal insulation and stress distribution are different.
3. The presence of thick ACPs has major consequences for planetary resurfacing in both the stagnant and the episodic lid regime, as they locally suppress volcanic activity. The surface age and crustal thickness distribution becomes more dichotomous: old, thin crust on the ACPs in contrast to the young, thick crust away from the plateaus. This is unlike the observations for Venus, where the surface age appears closer to uniform. The impact of ACPs depends on their size and thickness, of which thickness in particular is poorly constrained.
4. While episodic overturns may be regional without ACPs and up to 1/3 of thick preoverturn crust may be preserved, the presence of thick ACPs typically enforces global overturns away from the ACP, especially for higher yield stresses. However, parts of the preoverturn surface may be preserved at the trailing edge of the ACP due to the initiation of a spreading center close to the ACP. Other parts of the surface may also survive when the laterally moving ACP overrides a zone of subduction and enforces the premature cessation of crustal recycling.
5. Tessera regions are probably not well represented by the preimposed ACPs, as they likely feature less extreme age and crustal thickness contrasts than the modeled ACPs. The surviving non-ACP sections of the surface may be a closer approximation to tesserae, as these contrasts are much more moderate.

## Appendix A.

Physical parameters used for the model setup are shown in Table 1.

**Table A1**

*Physical Parameters Used for the Model Setup*

Physical parameter	Value	Dimension
Planetary radius	$6.052 \times 10^6$	m
Core radius	$3.186 \times 10^6$	m
Mantle thickness	$2.866 \times 10^6$	m
ACP thickness	$2.310 \times 10^5$	m
Surface temperature	740	K
CMB temperature	3,870	K
Super adiabatic temperature drop	2,300	K
Gravitational acceleration	8.87	$\text{m s}^{-2}$
Internal heating rate	$5 \times 10^{-12}$	$\text{W kg}^{-1}$
Mantle reference viscosity	$3 \times 10^{20}$	Pa s
Mantle density	3,378	$\text{kg m}^{-3}$
Mantle thermal expansivity	$2 \times 10^{-5}$	$\text{J mol}^{-1}$
Mantle thermal conductivity	4	$\text{W m}^{-1} \text{K}^{-1}$
Activation energy	$2 \times 10^5$	$\text{J mol}^{-1}$
Activation volume	$3.5 \times 10^{-6}$	$\text{m}^3 \text{mol}^{-1}$
Mantle specific heat capacity	1,250	$\text{J kg}^{-1} \text{K}^{-1}$
Latent heat of melting	$6 \times 10^5$	$\text{J kg}^{-1}$
Claperyron slope (ol system)	$(-2,2) \times 10^6$	$\text{Pa K}^{-1}$
Clapeyron slopes (px system)	$(1,1,0) \times 10^6$	$\text{Pa K}^{-1}$
Density jumps (ol system)	(150, 250)	$\text{kg m}^{-3}$
Density jumps (px system)	(150, 150, 250)	$\text{kg m}^{-3}$

Note. The mantle reference viscosity is defined at a reference temperature of 1,613 K and a reference pressure of 0 Pa.

## Data Availability Statement

Computations were performed on Stallo, a Notur facility at the University of Tromsø (Project Code: nn9010/ns9010). The used code StagYY (Tackley, 2008) is property of ETH Zürich and Paul J. Tackley and is available for collaborative studies from Paul J. Tackley. All data supporting our conclusions in this study can be obtained from Zenodo Data Repository (DOI: 10.5281/zenodo.3946779).

## Acknowledgments

This work originates from the MSc thesis of Rebecca Vilde Martine Krohn Karlsson at the Centre for Earth Evolution and Dynamics (CEED). Funding has been received from the Norwegian Research Council through a Centre of Excellence grant (CEED, 223272). This work was further supported by funding for the Norwegian Research School on Dynamics and Evolution of Earth and Planets (Project Number 249040/F60). T. R. acknowledges funding from the Norwegian Research Council through a Young Talents grant (PLATONICS, 276032).

## References

- Anderson, F. S., & Smrekar, S. E. (2006). Global mapping of crustal and lithospheric thickness on Venus. *Journal of Geophysical Research*, 111, E08006. <https://doi.org/10.1029/2004JE002395>
- Armann, M., & Tackley, P. J. (2012). Simulating the thermochemical magmatic and tectonic evolution of Venus's mantle and lithosphere: Two-dimensional models. *Journal of Geophysical Research*, 117, E12003. <https://doi.org/10.1029/2012JE004231>
- Basilevsky, A. T., Shalygin, E. V., Titov, D. V., Markiewicz, W. J., Scholten, F., Roatsch, T., et al. (2012). Geologic interpretation of the near-infrared images of the surface taken by the Venus Monitoring Camera, Venus Express. *Icarus*, 217(2), 434–450. <https://doi.org/10.1016/j.icarus.2011.11.003>
- Bindschadler, D. L., & Head, J. W. (1991). Tessera terrain, Venus: Characterization and models for origin and evolution. *Journal of Geophysical Research*, 96(B4), 5889–5907. <https://doi.org/10.1029/90JB02742>
- Bjornnes, E. E., Hansen, V. L., James, B., & Swenson, J. B. (2012). Equilibrium resurfacing of Venus: Results from new Monte Carlo modeling and implications for Venus surface histories. *Icarus*, 217(2), 451–461. <https://doi.org/10.1016/j.icarus.2011.03.033>
- Brown, C. D., & Grimm, R. E. (1997). Tessera deformation and the contemporaneous thermal state of the plateau highlands, Venus. *Earth and Planetary Science Letters*, 147(1–4), 1–10. [https://doi.org/10.1016/S0012-821X\(94\)00007-1](https://doi.org/10.1016/S0012-821X(94)00007-1)
- Buiter, S. J., & Torsvik, T. H. (2014). A review of Wilson cycle plate margins: A role for mantle plumes in continental break-up along sutures? *Gondwana Research*, 26(2), 627–653. <https://doi.org/10.1016/j.jgr.2014.02.007>
- Cramer, F. (2017). StagLab, Zendo, <https://doi.org/10.5281/zenodo.1199037>
- Cramer, F. (2018). Geodynamic diagnostics, scientific visualisation and StagLab 3.0. *Geoscientific Model Development*, 11(6), 2541–2562. <https://doi.org/10.5194/gmd-11-2541-2018>
- Cramer, F., Tackley, P., Meilick, I., Gerya, T., & Kaus, B. (2012). A free plate surface and weak oceanic crust produce single-sided subduction on Earth. *Geophysical Research Letters*, 39, L03306. <https://doi.org/10.1029/2011GL050046>
- Davaille, A., Smrekar, S. E., & Tomlinson, S. (2017). Experimental and observational evidence for plume-induced subduction on Venus. *Nature Geoscience*, 10(5), 349–355. <https://doi.org/10.1038/ngeo2928>
- Gerya, T. V., Connolly, J. A., & Yuen, D. A. (2008). Why is terrestrial subduction one-sided? *Geology*, 36(1), 43–46. <https://doi.org/10.1130/G24060A.1>

- Ghail, R. (2015). Rheological and petrological implications for a stagnant lid regime on Venus. *Planetary and Space Science*, 113–114, 2–9. <https://doi.org/10.1016/j.pss.2015.02.005>
- Ghent, R., & Hansen, V. (1999). Structural and kinematic analysis of eastern Ovda Regio, Venus: Implications for crustal plateau formation. *Icarus*, 139(1), 116–136. <https://doi.org/10.1006/icar.1999.6085>
- Ghent, R. R., Phillips, R. J., Hansen, V. L., & Nunes, D. C. (2005). Finite element modeling of short-wavelength folding on Venus: Implications for the plume hypothesis for crustal plateau formation. *Journal of Geophysical Research*, 110, E11006. <https://doi.org/10.1029/2005JE002522>
- Gillmann, C., & Tackley, P. (2014). Atmosphere/mantle coupling and feedbacks on Venus. *Journal of Geophysical Research: Planets*, 119, 1189–1217. <https://doi.org/10.1002/2013JE004505>
- Gilmore, M. S., Collins, G. C., Ivanov, M. A., Marinangeli, L., & Head, J. W. (1998). Style and sequence of extensional structures in tessera terrain, Venus. *Journal of Geophysical Research*, 103(E7), 16,813–16,840. <https://doi.org/10.1029/98JE01322>
- Guerrero, J., Lowman, J. P., Deschamps, F., & Tackley, P. (2018). The influence of curvature on convection in a temperature-dependent viscosity fluid: Implications for the 2-D and 3-D Modeling of moons. *Journal of Geophysical Research: Planets*, 123, 1863–1880. <https://doi.org/10.1029/2017JE005497>
- Guillou, L., & Jaupart, C. (1995). On the effect of continents on mantle convection. *Journal of Geophysical Research*, 100(B12), 24,217–24,238. <https://doi.org/10.1029/95JB02518>
- Hansen, V. L. (2018). Global tectonic evolution of Venus, from exogenic to endogenic over time, and implications for early Earth processes. *Philosophical Transactions of the Royal Society A - Mathematical Physical and Engineering Sciences*, 376(2132), 20170412. <https://doi.org/10.1098/rsta.2017.0412>
- Hansen, V. L., Phillips, R. J., Willis, J. J., & Ghent, R. R. (2000). Structures in tessera terrain, Venus: Issues and answers. *Journal of Geophysical Research*, 105(E2), 4135–4152. <https://doi.org/10.1029/1999JE001137>
- Hashimoto, G. L., Roos-Serote, M., Sugita, S., Gilmore, M. S., Kamp, L. W., Carlson, R. W., & Baines, K. H. (2008). Felsic highland crust on Venus suggested by Galileo Near-Infrared Mapping Spectrometer data. *Journal of Geophysical Research*, 113, E00B24. <https://doi.org/10.1029/2008JE003134>
- Hernlund, J. W., & Tackley, P. J. (2008). Modeling mantle convection in the spherical annulus. *Physics of the Earth and Planetary Interiors*, 171(1–4), 48–54. <https://doi.org/10.1016/j.pepi.2008.07.037>
- Ivanov, M. A., & Basilevsky, A. T. (1993). Density and morphology of impact craters on tessera terrain. *Geophysical Research Letters*, 20(23), 2579–2582. <https://doi.org/10.1029/93GL02692>
- Ivanov, M. A., & Head, J. W. (2011). Global geological map of Venus. *Planetary and Space Science*, 59(13), 1559–1600. <https://doi.org/10.1016/j.pss.2011.07.008>
- James, P. B., Zuber, M. T., & Phillips, R. J. (2013). Crustal thickness and support of topography on Venus. *Journal of Geophysical Research: Planets*, 118, 859–875. <https://doi.org/10.1029/2012JE004237>
- Johnson, T. E., Brown, M., Kaus, B. J., & VanTongeren, J. A. (2014). Delamination and recycling of Archaean crust caused by gravitational instabilities. *Nature Geoscience*, 7(1), 47–52. <https://doi.org/10.1038/ngeo2019>
- Kargel, J., Komatsu, G., Baker, V., & Strom, R. (1993). The volcanology of Venera and VEGA landing sites and the geochemistry of Venus. *Icarus*, 103(2), 253–275. <https://doi.org/10.1006/icar.1993.1069>
- Kidder, J. G., & Phillips, R. J. (1996). Convection-driven subsolidus crustal thickening on Venus. *Journal of Geophysical Research*, 101(E10), 23,181–23,194. <https://doi.org/10.1029/96JE02530>
- King, S. D. (2018). Venus resurfacing constrained by geoid and topography. *Journal of Geophysical Research: Planets*, 123, 1041–1060. <https://doi.org/10.1002/2017JE005475>
- Kreslavsky, M. A., Ivanov, M. A., & Head, J. W. (2015). The resurfacing history of Venus: Constraints from buffered crater densities. *Icarus*, 250, 438–450. <https://doi.org/10.1016/j.icarus.2014.12.024>
- Lenardic, A., & Moresi, L. N. (1999). Some thoughts on the stability of cratonic lithosphere: Effects of buoyancy and viscosity. *Journal of Geophysical Research*, 104(B6), 12,747–12,758. <https://doi.org/10.1029/1999JB900035>
- Lenardic, A., Moresi, L.-N., Jellinek, A., & Manga, M. (2005). Continental insulation, mantle cooling, and the surface area of oceans and continents. *Earth and Planetary Science Letters*, 234(3–4), 317–333. <https://doi.org/10.1016/j.epsl.2005.01.038>
- Lenardic, A., Moresi, L. N., & Mühlhaus, H. (2003). Longevity and stability of cratonic lithosphere: Insights from numerical simulations of coupled mantle convection and continental tectonics. *Journal of Geophysical Research*, 108(B6), 2303. <https://doi.org/10.1029/2002JB001859>
- Lourenço, D. L., Rozel, A., & Tackley, P. J. (2016). Melting-induced crustal production helps plate tectonics on Earth-like planets. *Earth and Planetary Science Letters*, 439, 18–28. <https://doi.org/10.1016/j.epsl.2016.01.024>
- Lourenço, D. L., Rozel, A. B., Ballmer, M. D., & Tackley, P. J. (2020). Plutonic-squishy lid: A new global tectonic regime generated by intrusive magmatism on earth-like planets. *Geochemistry, Geophysics, Geosystems*, 21, e2019GC008756. <https://doi.org/10.1029/2019GC008756>
- Lourenço, D. L., Rozel, A. B., Gerya, T., & Tackley, P. J. (2018). Efficient cooling of rocky planets by intrusive magmatism. *Nature Geoscience*, 11(5), 322–327. <https://doi.org/10.1038/s41561-018-0094-8>
- McKinnon, W. B., Zahnle, K., Ivanov, B. A., & Melosh, H. J. (1997). Cratering on Venus: Modeling and observations. In W. Bougher, D. M. Hunten, R. J. Phillips (Eds.), *Venus II* (pp. 969–1014). Tucson: University of Arizona Press.
- Mitrovica, J., & Forte, A. (2004). A new inference of mantle viscosity based upon joint inversion of convection and glacial isostatic adjustment data. *Earth and Planetary Science Letters*, 225(1–2), 177–189. <https://doi.org/10.1016/j.epsl.2004.06.005>
- Moore, W. B., & Webb, A. A. G. (2013). Heat-pipe earth. *Nature*, 501(7468), 501–505. <https://doi.org/10.1038/nature12473>
- Noack, L., Breuer, D., & Spohn, T. (2012). Coupling the atmosphere with interior dynamics: Implications for the resurfacing of Venus. *Icarus*, 217(2), 484–498. <https://doi.org/10.1016/j.icarus.2011.08.026>
- Nunes, D. C., Phillips, R. J., Brown, C. D., & Dombard, A. J. (2004). Relaxation of compensated topography and the evolution of crustal plateaus on Venus. *Journal of Geophysical Research*, 109, E01006. <https://doi.org/10.1029/2003JE002119>
- Ogawa, M., & Yanagisawa, T. (2014). Mantle evolution in Venus due to magmatism and phase transitions: From punctuated layered convection to whole-mantle convection. *Journal of Geophysical Research: Planets*, 119, 867–883. <https://doi.org/10.1002/2013JE004593>
- Phillips, B. R., & Coltice, N. (2010). Temperature beneath continents as a function of continental cover and convective wavelength. *Journal of Geophysical Research*, 115, B04408. <https://doi.org/10.1029/2009JB006600>
- Roberts, K. M., Guest, J. E., Head, J. W., & Lancaster, M. G. (1992). Mylitta Fluctus, Venus: Rift-related, centralized volcanism and the emplacement of large-volume flow units. *Journal of Geophysical Research*, 97(E10), 15,991–16,015. <https://doi.org/10.1029/29JE01245>

- Rolf, T., Coltice, N., & Tackley, P. (2012). Linking continental drift, plate tectonics and the thermal state of the Earth's mantle. *Earth and Planetary Science Letters*, 351–352, 134–146. <https://doi.org/10.1016/j.epsl.2012.07.011>
- Rolf, T., Coltice, N., & Tackley, P. J. (2014). Statistical cyclicity of the supercontinent cycle. *Geophysical Research Letters*, 41, 2351–2358. <https://doi.org/10.1002/2014GL059595>
- Rolf, T., Steinberger, B., Sruthi, U., & Werner, S. C. (2018). Inferences on the mantle viscosity structure and the post-overturn evolutionary state of Venus. *Icarus*, 313, 107–123. <https://doi.org/10.1016/j.icarus.2018.05.014>
- Rolf, T., & Tackley, P. J. (2011). Focussing of stress by continents in 3D spherical mantle convection with self-consistent plate tectonics. *Geophysical Research Letters*, 38, L18301. <https://doi.org/10.1029/2011GL048677>
- Romeo, L., & Capote, R. (2011). Tectonic evolution of Ovda Regio: An example of highly deformed continental crust on Venus? *Planetary and Space Science*, 59(13), 1428–1445. <https://doi.org/10.1016/j.pss.2011.05.013>
- Romeo, L., & Turcotte, D. L. (2008). Pulsating continents on Venus: An explanation for crustal plateaus and tessera terrains. *Earth and Planetary Science Letters*, 276(1–2), 85–97. <https://doi.org/10.1016/j.epsl.2008.09.009>
- Romeo, L., & Turcotte, D. L. (2010). Resurfacing on Venus. *Planetary and Space Science*, 58(10), 1374–1380. <https://doi.org/10.1016/j.pss.2010.05.022>
- Rozel, A. B., Golabek, G. J., Jain, C., Tackley, P. J., & Gerya, T. (2017). Continental crust formation on early Earth controlled by intrusive magmatism. *Nature*, 545(7654), 332–335. <https://doi.org/10.1038/nature22042>
- Sandwell, D. T., & Schubert, G. (1992). Evidence for retrograde lithospheric subduction on Venus. *Science*, 257(5071), 766–770. <https://doi.org/10.1126/science.257.5071.766>
- Schaber, G. G., Strom, R. G., Moore, H. J., Soderblom, L. A., Kirk, R. L., Chadwick, D., et al. (1992). Geology and distribution of impact craters on Venus: what are they telling us? *Journal of Geophysical Research*, 97(E8), 13,257–13,301. <https://doi.org/10.1029/92JE01246>
- Shalygin, E. V., Markiewicz, W. J., Basilevsky, A. T., Titov, D. V., Ignatiev, N. I., & Head, J. W. (2015). Active volcanism on Venus in the Ganiki Chasma rift zone. *Geophysical Research Letters*, 42, 4762–4769. <https://doi.org/10.1002/2015GL064088>
- Smrekar, S., Stofan, E., Mueller, N. T., Treiman, A., Elkins-Tanton, L. T., Helbert, J., et al. (2010). Recent hotspot volcanism on Venus from VIRTIS emissivity data. *Science (New York, N.Y.)*, 328(5978), 605–608. <https://doi.org/10.1126/science.1186785>
- Steinberger, B., Werner, S. C., & Torsvik, T. H. (2010). Deep versus shallow origin of gravity anomalies, topography and volcanism on Earth, Venus and Mars. *Icarus*, 207(2), 564–577. <https://doi.org/10.1016/j.icarus.2009.12.025>
- Tackley, P. J. (2000). Self-consistent generation of tectonic plates in time-dependent, three-dimensional mantle convection simulations. *Geochemistry, Geophysics, Geosystems*, 1(8), 1021. <https://doi.org/10.1029/2000GC000036>
- Tackley, P. J. (2008). Modelling compressible mantle convection with large viscosity contrasts in a three-dimensional spherical shell using the yin-yang grid. *Physics of the Earth and Planetary Interiors*, 171(1–4), 7–18. <https://doi.org/10.1016/j.pepi.2008.08.005>
- Tackley, P. J., & King, S. D. (2003). Testing the tracer ratio method for modeling active compositional fields in mantle convection simulations. *Geochemistry, Geophysics, Geosystems*, 4(4), 8302. <https://doi.org/10.1029/2001GC000214>
- Turcotte, D. L. (1989). Fractals in geology and geophysics. *Pure and Applied Geophysics*, 131(1–2), 171–196. [https://doi.org/10.1007/978-3-0348-6389-6\\_10](https://doi.org/10.1007/978-3-0348-6389-6_10)
- Wei, D., Yang, A., & Huang, J. (2014). The gravity field and crustal thickness of Venus. *Science China Earth Sciences*, 57(9), 2025–2035. <https://doi.org/10.1007/s11430-014-4824-5>
- Weller, M. B., & Kiefer, W. S. (2019). The physics of changing tectonic regimes: Implications for the temporal evolution of mantle convection and the thermal history of Venus. *Journal of Geophysical Research: Planets*, 125, e05960. <https://doi.org/10.1029/2019JE005960>
- Wroblewski, F. B., Treiman, A. H., Bhiravarasu, S., & Gregg, T. K. (2019). Ovda Fluctus, the Festoon lava flow on Ovda Regio, Venus: Not silica-rich. *Journal of Geophysical Research: Planets*, 124, 2233–2245. <https://doi.org/10.1029/2019JE006039>
- Xie, S., & Tackley, P. J. (2004). Evolution of U-Pb and Sm-Nd systems in numerical models of mantle convection and plate tectonics. *Journal of Geophysical Research*, 109, B11204. <https://doi.org/10.1029/2004JB003176>
- Yoshida, M. (2008). Mantle convection with longest-wavelength thermal heterogeneity in a 3-D spherical model: Degree one or two? *Geophysical Research Letters*, 35, L23302. <https://doi.org/10.1029/2008GL036059>
- Yoshida, M. (2010). Temporal evolution of the stress state in a supercontinent during mantle reorganization. *Geophysical Journal International*, 180(1), 1–22. <https://doi.org/10.1111/j.1365-246X.2009.04399.x>